HEAVY PRECIPITATION FROM HURRICANE LANE ON HAWAIʻI ISLAND

A THESIS SUBMITTED TO THE GRADUATE DIVISION OF THE
UNIVERSITY OF HAWAIʻI AT MĀNOA IN PARTIAL FULFILLMENT
OF THE REQUIREMENTS FOR THE DEGREE OF

MASTER OF SCIENCE

IN

ATMOSPHERIC SCIENCES

JUNE 2019

By
Gavin T. Shigesato

THESIS COMMITTEE:

Alison D. Nugent, Chairperson
Yi-Leng Chen
Thomas Giambelluca

ACKNOWLEDGMENTS

I would like to thank many people for the accomplishment of my thesis. I am very thankful for my adviser Alison Nugent who provided me an opportunity to seek out my interest of Hurricane Lane under her guidance. Her patience and willingness to improve my coding skills, research process, and my scientific thinking is something I am grateful for. Providing the helpful codes to process different files and to analyze them. Without her experience, constructive criticism in my data analysis and writing, having group meetings, the flexibility to meet with me, and her own expertise in mountain meteorology and coding, this project would not be possible. I would also like to thank my committee members, Yi-Leng Chen, and Thomas Giambelluca for their helpful comments and constructive criticism which challenged me to further improve my research. Both provided a lot of value into creating a thesis that I am proud of. In addition, Yi-Leng Chen's masters classes provided a foundation to learn upon in the weather in Hawai‘i.

I would also like to the Department of Atmospheric Sciences at the University of Hawai‘i at Mānoa for providing me with partial financial support as an undergraduate and masters student. Also, my fellow classmates and friends who provided me with feedback and spending their own time to proofread my drafts. My time at UH has provided me with valuable skills in the thinking process and knowledge to continue my career in atmospheric sciences.

Also, the LROSE team who helped process and work out the different LROSE applications. Thank you to Mike Dixon for providing the large data files in order to analyze the radar data.

Furthermore, the entire National Weather Service Forecast Office in Honolulu for providing me the opportunity to continue my graduate degree while working full time for them. Thankful for the rain gauge data, the knowledge of weather in Hawai‘i, the support in coming to see my seminar and presentation by providing feedback to improve my research, and their patience while on shift work to let me meet with my advisor. Also to the many forecasters and

management personnel for answering the numerous questions that I had regarding the radar, rain gauges, and background information to make this thesis the best it can be.

I would like to thank my friends and family whose constant support kept the motivation and belief to attain a Masters degree. Time spent with them during study breaks at Bale, and days off at the beach kept me sane and their support in this thesis was invaluable. Finally, I would like to thank my parents and Shannon Lee for the daily support throughout the academic journey. Without them, these past 2 years in the graduate program would have been much longer then they were.

ABSTRACT

Hurricane Lane (2018) significantly impacted the Hawaiian Islands, bringing heavy rainfall and widespread flooding especially to Hawai‘i Island. Rain gauges measured > 1270 mm of rainfall on the windward slopes of Hawai‘i Island over four days. In this study, an 8-hr period during an early part of the storm was analyzed. This period was chosen because winds were primarily easterly. Thus this time period serves as an extreme case for the typical trade wind flow and the precipitation pattern associated with it on Hawai‘i Island. An analysis of several observational datasets of the storm environment and the resulting precipitation provides strong evidence for orographic enhancement during the early part of Hurricane Lane’s impacts on the Hawaiian Islands. Lane was an ideal case study for understanding the factors that lead to heavy rainfall in Hawai‘i, and acts as a proxy for understanding high rainfall events.

TABLE OF CONTENTS

List of Figures ‘

1. INTRODUCTION

Hurricane Lane (2018) was an impactful event for the State of Hawai‘i, in particular Hawai‘i Island. It brought extreme rainfall, with 1,270 mm (50”) over a period of four days, to the windward slopes of Hawai’i Island, a region already accustomed to high annual rainfall totals. Much of the eastern portion of Hawai‘i Island typically receives over 2,000 mm (79”) of rainfall every year, with some of those portions receiving over 7 m (276”) (Giambelluca 2013).

Extreme rainfall can result from long-duration light rain, short-duration heavy rain, or a combination of the two. As defined in the literature, a ‘heavy’ rainfall event for a specific location exceeds 50.8 mm (2”) in a 24-h time period (Karl et al. 1996; Groisman et al. 1999). A ‘very heavy’ rainfall event exceeds 101.6 mm (4”) in a 24-h time period. The rainfall from Lane well exceeds the very heavy rainfall criteria four days in a row making it both long-duration and heavy. Unsurprisingly, the extreme rainfall from Lane caused damage to roads and infrastructure, as well as widespread flooding to the windward side of Hawai‘i island.

A majority of rainfall in Hawai‘i comes in the winter months (October-March), known as the wet-season, from cold fronts, Kona Lows, and upper-level troughs. Extratropical weather systems can propagate sufficiently equatorward to substantially alter the dominant, stable trade wind pattern in the vicinity of the Hawaiian Islands (Businger and Birchard 1997). In contrast, the summer months (April-September) are known as the dry-season. The dry-season is defined by smaller total rainfall accumulations as well as less frequent heavy rainfall events (Bier et al. 1983). Perhaps the only exception is tropical disturbances, which can produce anomalously high rainfall during the dry-season. Tropical storms in the Central Pacific occur during the Hurricane season, extending from June 1st through November 30th, overlapping with the end of the dry-season. Tropical systems often form in lower latitudes of the eastern Pacific and move westward into the central Pacific region. On average, one tropical system of depression strength or greater passes within 300 km of the Hawaiian Islands every two years (Kodama and Barnes 1997).

Heavy rainfall in the Hawaiian Islands is typically associated with 1) the slopes facing the prevailing low level winds, 2) nighttime hours, 3) thunderstorms were associated with heavy rainfall events, and 4) an upper-tropospheric trough axis to the west of the state (Haraguchi 1977), all common features associated with heavy rainfall in the tropics (Maddox et al. 1979). Heavy rainfall in Hawai‘i is not uncommon; within the last decade heavy rainfall events have occurred across all islands. Three past events highlighting the four factors from Haraguchi (1977) are discussed below.

On April 13-15 2018, flash flooding occurred on both Kaua‘i and O‘ahu. An upper level low tapped into enhanced moisture embedded with the low level trade winds, producing extreme rainfall totals. A rain gauge at Waipa on the north side of Kaua‘i measured 1262 mm of rain in a 24-h period. This exceeded a “very heavy” rainfall event by over 1000% and included factors 1, 3 and 4.

In 2014, tropical storm Iselle made landfall on Hawai‘i island as the first tropical cyclone to make landfall in the State since 1992. During the event, Iselle produced rainfall across the entire island chain but most fell on the east and southeast facing slopes of Hawai‘i Island. The slopes facing the prevailing low level winds received 150 mm to 250 mm of rain over a 4-day period. One station 25 miles west of Hilo measured a total of 387 mm over the course of four days. Rainfall over the 4-day event could be characterized as “heavy” during different 24-h periods and was a result of factors 1 and 3.

Finally, on June 4, 2011, an upper level low pressure produced an unstable air mass over O‘ahu with frequent thunderstorms and lightning. The upper level low removed the stabilizing inversion allowing deep convection to develop. On this day, a rain gauge on the windward side of O‘ahu measured over 398 mm in a 6-h duration. The heavy rainfall was associated with thunderstorms and an upper-tropospheric trough axis west of the state (factors 3 and 4). With high rainfall totals in a 6-h period, this event exceeds the “very heavy” rainfall event by over 300% just in those six hours.

This study focuses on Hurricane Lane (2018, hereafter simply Lane) which provided long-duration moist low-level flow for the slopes facing the prevailing low level wind on

Hawai‘i Island (factor 1). This aspect, among others, played a role in producing the 3rd highest rainfall total in the U.S. from a tropical cyclone since 1950 (Hawai‘i RR5HFO summary).

Hawai‘i Island is the largest island in the Hawaiian chain, boasting mountainous terrain with two volcanic mountains exceeding 4 km in elevation. Due to the nature of the low-level flow impinging on the windward slopes of Hawai‘i Island, it is hypothesized that precipitation from Lane was orographically enhanced. Forced mechanical lifting of the air on the windward slopes of mountains leads to cooling of the air column, resulting in condensation and precipitation (Roe 2005). The stronger the upslope flow, the higher the moisture flux and stronger the upward forcing for clouds and precipitation (Kodama and Barnes 1997). Previous studies on the Hawaiian Islands done by Nullet and McGranaghan (1998), has shown that Hawai‘i Island rainfall is enhanced 2.5 times that of open ocean values.

Orographic enhancement of hurricane precipitation has been noted before (e.g. Smith et al. 2009; Dehart and Houze 2017) and depends on the relative orientation of the airflow and topography, the specific region of the storm encountering the terrain, and many other event-specific factors that vary in time and space (Dehart and Houze 2017). Upstream of mountain ranges with sufficient height and width in the direction of flow, surface rainfall can maximize on the windward slope (Yu and Cheng 2008,2013).

Houze (2012) discusses many possible mechanisms of orographic enhancement (Figure 1). Figure 1a refers to the case in which the air approaching a barrier is stable and generally follows the terrain upward, and the vertical component of the motion produces or strengthens a cloud on the windward (Houze 2012). Figure 1b is similar to figure 1a, although the flow is unstable. Figure 1d shows schematically how nighttime cooling over the higher terrain suppresses convection on a mountaintop. Figure 1e depicts a case where a preexisting cloud passing over a hill or small mountain is enhanced to produce a maximum of precipitation on the upwind side of the barrier, but the hill is low enough in altitude that the precipitating cloud is advected over to the lee side, where its precipitating capacity is weakened by the downslope air motion (Houze 2012). Figure 1f is a mechanism called “seeder-feeder” has been shown to amplify precipitation over terrain in storm environments (Smith et al. 2009; Bergeron 1950, 1968). This happens when a pre-existing precipitation cloud is advected over a hill, while

directly over the hill a shallow orographic cloud forms over the low level slope (Houze 2012). Precipitation particles from the upper cloud (seeder) grow by accretion of cloud water in the lower cloud (feeder). This enhances the precipitation on the windward side of the mountain (Bergeron 1965). Therefore, the location of rainfall in a tropical cyclone over mountainous terrain is dictated by orographic geometry, microphysical processes, and cyclone kinematics (Dehart and Houze 2017).

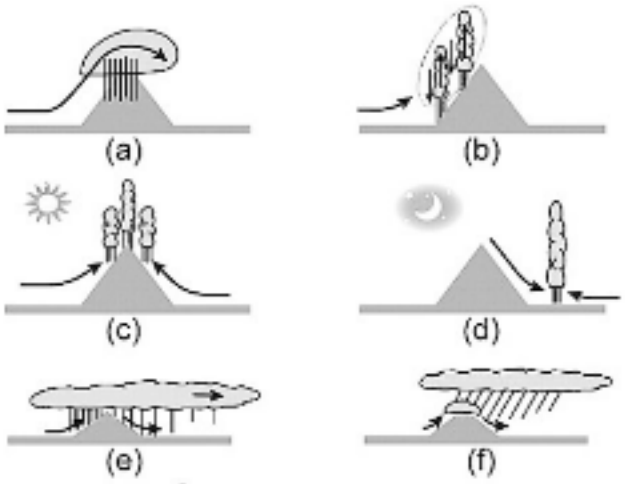

Figure 1: Mechanisms by which mountains and hills affect precipitating clouds. a) stable flow over mountain b) unstable flow c) daytime upslope flow d) nighttime katabatic down slope flow e) orographic enhancement of pre-existing rainfall f) seeder feeder mechanism (from Houze 2012).

With this in mind, it is vital to learn from Lane how local island orography affects precipitation in those storm systems. Nearly 18% of the average climatological rainfall occurred in a 4 day period, on Hawai‘i Island, during Lane. The extreme flooding that damaged property and threatened lives over the windward side of Hawai‘i Island was the driving force in investigating the precipitation in this area. Numerous studies on Hawai‘i Island have looked at precipitation from normal trade wind flow, Kona Lows, and other weather events that occur throughout the year. Due to the rarity of an event like Lane, I examined the location of extreme

precipitation accumulations to learn more about the orographic effects and why the rainfall was significantly enhanced over this area and less elsewhere. Through multiple observational datasets which included radar and rain gauges, I hypothesized that different upslope mechanisms, terrain enhancement, and the location of Lane's rainbands brought the high rainfall totals in an area south of Hilo.

2. METHODS

a. Data Collection

A combination of observational datasets and weather service products were used to understand the precipitation from Hurricane Lane. The datasets and methods are described below.

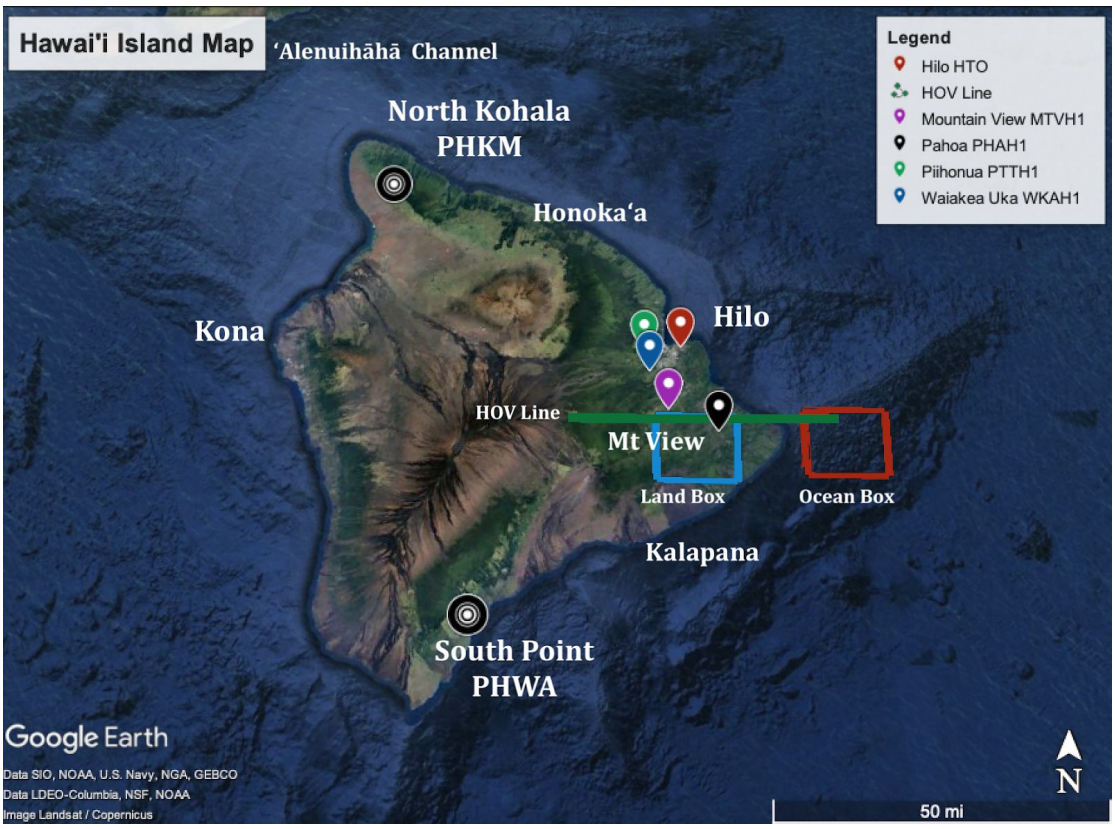

Figure 2:Hawai'i Island Map including city and geographic names, the locations of two radars (PHKM and PHWA, black circles), an ocean box (red outline) and a land box (blue outline) used for analysis. A line used for a Hovmoller diagram (green) is 69.04 km long along 19.5468 °N from 155.3293 - 154.6715 °W. A few specific rain gauge locations are marked including Hilo (HTO 19.72 °N 155.04 °W*, red), Pi'ihounua (PTTH1 19.7098* °N 155.139 °W*, green), Mountain View (MTVH1 19.5490* °N 155.1101 °W*, purple), Waikea Uka (WKAH1 19.658* °N 155.1277 °W*, blue), and Pahoa (PHAH1, black).*

i. Hurricane Advisories

The National Hurricane Center provided track and forecast guidance from genesis until Lane traversed 140°W on August 18, 2018. Afterward, the Central Pacific Hurricane Center provided forecast and advisory packages every six hours which included the strength and position of Lane.

ii. Radars

NEXRAD radar from South Kauaʻi (PHKI), Molokaʻi (PHMO), South Point (PHWA) and North Kohala radar on Hawaiʻi Island (PHKM) were used to analyze precipitation from Lane (Figure 3). The four radars are S-band doppler radars and provide rainfall estimates both onshore and offshore.

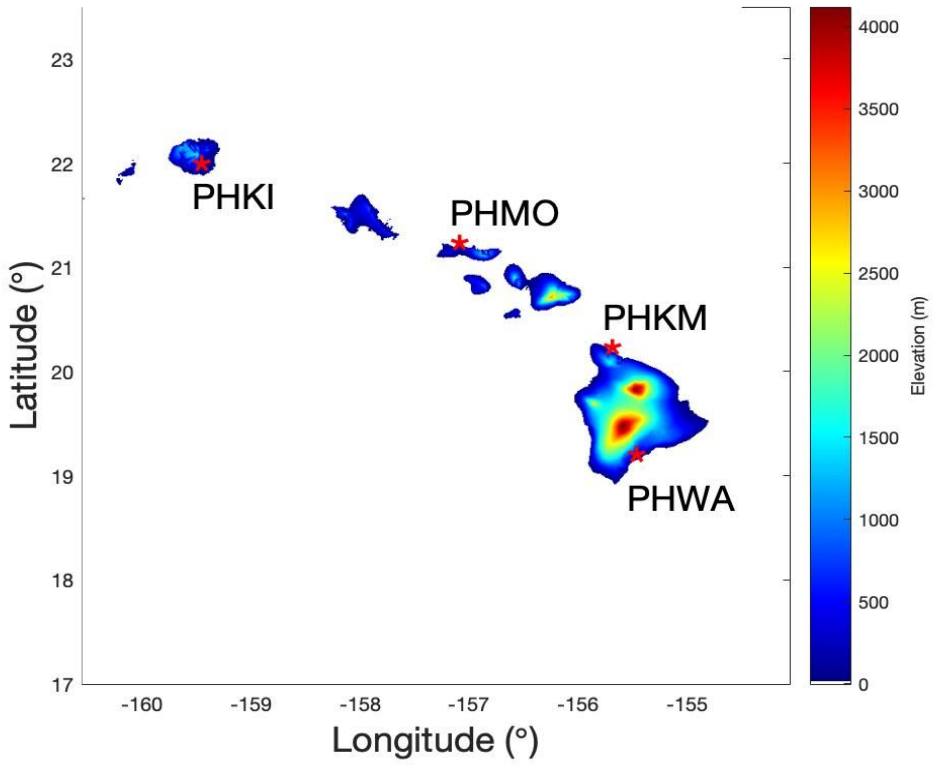

Figure 3: Four NEXRAD WSR 88D S-Band radars located across the islands indicated by the red asterisks (*) overlaid on the terrain (m) of the Hawaiian Islands.

The volume coverage pattern (VCP) mode used during Lane was VCP 121. This mode is capable of rapid volume sampling of nine elevation angles in about 5.75 minutes (Secretaries of Commerce). While the vertical resolution is lacking, it scans the lower levels multiple times and in different pulse repetition frequencies. The result of this VCP is enhanced velocity data. VCP

121 provides base data with far less range overlaid echoes and velocity aliased data and is recommended for sampling widespread non-severe echo coverage and hurricanes that are still offshore when viewing large scale structures is the priority (Secretaries of Commerce et al. 2014).

iii. Rain Gauges

Telemetered tipping-bucket rain gauges from the rainfall network Longman et al. (2018, Scientific Data), and the Hydronet database with the National Weather Service (NWS) Honolulu Forecast office (HFO) were also used to analyze rainfall from time series accumulations. A total of 52 sites spread across Hawai‘i Island with at least 15-min temporal resolution were utilized (eight stations had 5-min temporal resolution). The gauges of 5-min temporal resolution use a tipping bucket mechanism with an accuracy of 1.5% in the 0-150 mm hr^{-1} range.

iv. Other Observations

Wind measurements from different data sets across Hawai‘i Island were used to observe wind speed and direction. Wind stations, radiosonde balloon soundings, and reanalysis data from the ECMWF were used. The wind stations used were located in Honoka‘a, Hilo, and two near Kalapana (Figure 2).

Radiosonde balloon soundings were also used from the Hilo site that were launched at a 6-h frequency during Lane at 00z, 06z, 12z, and 18z for the duration of the storm. These observations provided information about the vertical structure of the atmosphere, and another method to observe wind speed and direction.

Offshore wind observations from ECMWF IFS CY41r2 model upstream were also taken to represent the environmental flow not affected by terrain. This reanalysis observation was used to find the average wind direction and speed at 925 mb in a gridded box upstream of Hawai‘i Island.

b. Analysis Methods

i. LROSE

The Lidar Radar Open Software Environment (LROSE) developed at NCAR was used to analyze the radar data. LROSE converts raw NEXRAD data to radar derived variables; in this study the radar derived variables are used to calculate the precipitation rate, and the qualitative precipitation estimates (QPE).

The process to get the QPE takes a few steps. First, raw NEXRAD level II data is used to estimate the specific differential phase (KDP) using a modified version of the Hubbert FIR filter method (Hubbert et al. 1993). KDP shows the change in differential phase shift. Simply, positive KDP values indicate an increase in the size and concentration of rain drops, and thus, an increase in rain rate. Next, particle identification (PID) is derived from KDP. Radiosonde balloon soundings from Lihue and Hilo were used to estimate the 0°C isotherm, crucial in deriving PID. The modified NCAR fuzzy-logic-based PID algorithm for S-band polarimetric radar was used to process the data and estimate the particle types during each radar scan (Vivekandan et al 1999). One of 16 PIDs are chosen for each grid point . The nearest sounding in time and space is used for each radar and radar scan.

Finally, precipitation is estimated in 3D; five independent estimates are used to derive different estimates of rain rate. In LROSE, they are known as ‘rate zh’,‘rate z zdr’,‘rate kdp’,‘rate pid’, and ‘rate hybrid’. The rate used in this study is ‘rate hybrid’ and is based on the PID and Bringi algorithm by Bringi et al. (2001). Note that it is a more accurate rain rate estimate than the classic ZR relationship because it takes into account the particle type rather than just the reflectivity. Due to frozen precipitation of various types (graupel, snow, ice etc.) identifying the particles gives more accurate rain rates.

Due to the mountainous terrain across the Hawaiian Island chain, beam blockage is important to consider when deriving QPE. A beam block algorithm uses 30 m vertical resolution terrain data and produces a beam blockage file containing blocked percentage for each elevation angle spaced at 0.2° (Bringi et al. 2001). If a range gate has <25% blockage, it is treated as

unblocked and used for precipitation estimation. If the blockage >25%, the next highest elevation angle is used. The 25% threshold was chosen because with 75% of the power available, the computed reflectively will only be reduced by 1.2 dB, so any incurred errors will be moderate.

Beam blockage maps at two elevations and two locations are shown in Figure 4. The radar in South Point of Hawai‘i Island is unable to see the north side of the island due to the high terrain blocking its view (Fig 3 top row). Similarly, the radar in North Kohala of Hawai‘i Island is unable to see the south side of the island due to the high terrain blocking its view (Figure 4 bottom row). Note the different percentages of beam blockage on the east side of the island at different elevations.

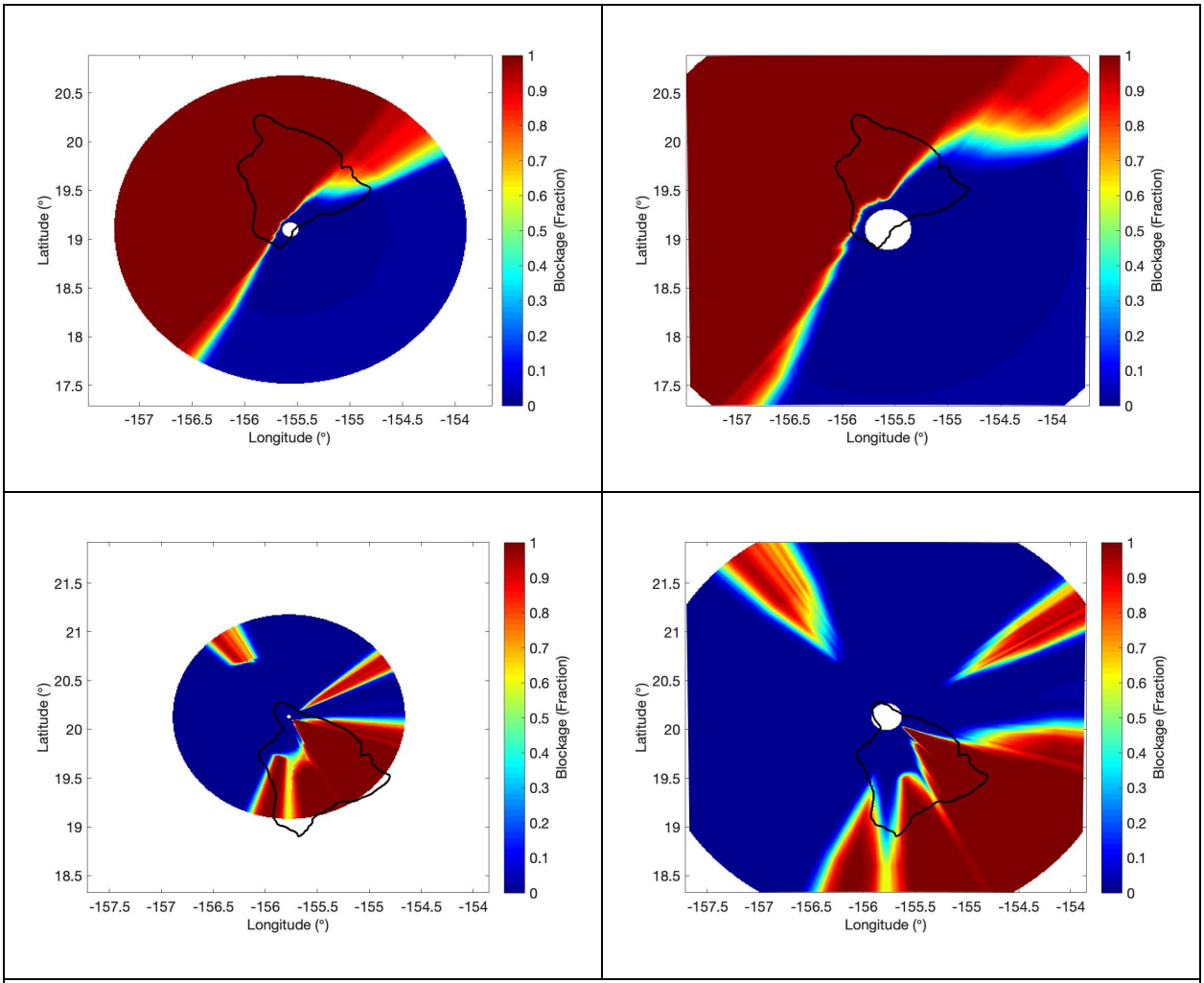

Figure 4: Beam blockage (fraction) due to terrain from the South Point (PHWA, top row) and

North Kohala (PHKM, bottom row) radar at 1.5 km (left) and 3.5 km (right) scan levels.

KDP, PID, and rain rate, were derived for each single scan on the radar to quantify rainfall accumulations throughout the Lane event. QPE from each radar (PHKI, PHMO, PHMK, and PHWA) was merged to create a full Hawaiian Island map of rain accumulation. Where overlap of radar coverage occurs, the closest radar's nonzero value is chosen. Analysis using radar is focused on the relative differences/patterns rather than the absolute values.

ii. Radar Analysis

The primary advantage of the radar as compared with a rain gauge is the ability to observe areas over land and areas over the ocean. The following analyses are used after the data has been processed through LROSE.

iii. Box Comparisons

Time series of offshore and onshore precipitation were produced from the radar data using the average accumulated rainfall in a land box and an ocean box (Figure 2) to compare rainfall over time. The land box is located on the southeast side of Hawai‘i Island from 19.4026-19.5554 °N and from 154.9188-155.1179 °W. The ocean box was located to the east and offshore from 19.5677-19.4149 °N and from 154.7553-154.5562 °W.

Iv. Hovmoller

Hovmoller (abbreviated as Hov) diagrams are used to interpret rain rate through time along a latitudinal line. Using the hovmoller changes in rain rate of individual precipitating cells as they move onshore from east to west were observed. The Hovmoller latitudinal line used is 69.04 km (42.9 miles) in length, at 19.5468 °N from 155.3293 - 154.6715 °W, as shown in Figure 2.

v. Vertical Cross Sections

Vertical cross-sections of reflectivity in a quasi Range Height Indicator (RHI) view are used to observe how the altitude and vertical structure of a precipitating cell changed through time.

3. RESULTS

a. Hurricane Lane Overview

Tropical Depression Fourteen-E formed on August 14, 2018 at 2000 UTC. The system was forecast to move primarily westward and strengthen. On August 16, the storm system strengthened to a Category 1 hurricane and was named Lane. With a well-defined inner core and a partial eye, Lane showed a strong chance of intensifying into a major hurricane, especially as the storm was forecast to move into an area with low wind shear and warm sea surface temperatures (SST). Sure enough, Lane continued to track westward (Figure 5), steered by the trade winds on the south of the subtropical high and on August 18 Lane entered the Central Pacific as a Category 4 hurricane.

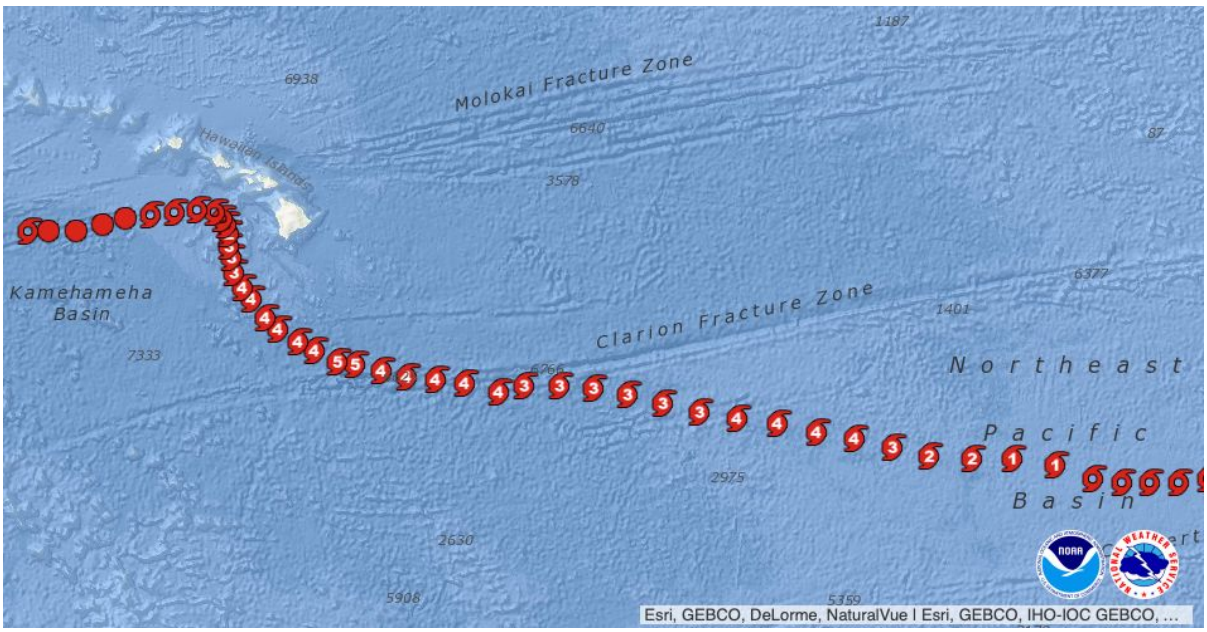

Figure 5: The track of Hurricane Lane from August 16-28, 2018. The hurricane symbols show the location of the storm center along with the Category (from: http://www.prh.noaa.gov/cphc/tcpages/latest_gis.php?stormid=EP142018).

With SSTs above 27°C and only 10-15 kts of vertical wind shear, Lane strengthened to a Category 5 by August 21. Lane had been moving generally westward along the southern flank of a mid-level ridge, but as it reached Category 5 strength, it rounded the western periphery of the ridge and moved into an area of low steering flow. This caused Lane to turn northward slowly. Lane moved north into the coastal waters of the State of Hawai‘i on August 22. Hawai‘i Island began feeling impacts from Lane as early as August 22 as the outer bands of Lane came ashore on the windward side of Hawai‘i Island.

Lane weakened to a Category 4 storm when it was about 458 km south of Kailua Kona. Facing strong shear of 18-20 m s^{-1}, the low level circulations of Lane decoupled (Ballard 2018) and was predicted to weaken throughout the following 48 hrs. Lane stalled southwest of Hawai‘i Island as the outer rainbands continued to pull tropical air over the windward slopes for the next four days. Finally, Lane weakened due to the high shear environment and drifted westward on August 26, 2018.

Due to Lane's position south of the Hawaiian islands and its counter-clockwise rotation, the synoptic wind direction affecting the windward side of Hawai'i Island was generally east from 45-150° throughout the 2-day period from August 22 to 23. On August 24 and 25, wind station data from the sounding and stations near Kalapana, shows the winds on Hawai'i Island turned to the northeast, and later became light and variable (not shown).

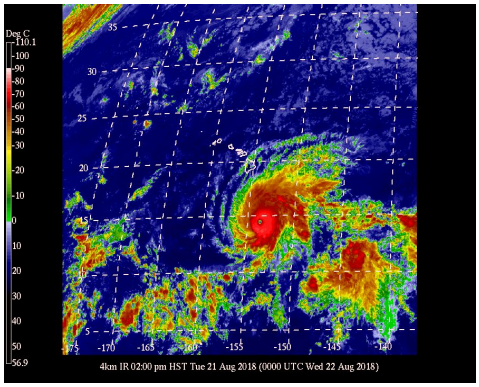

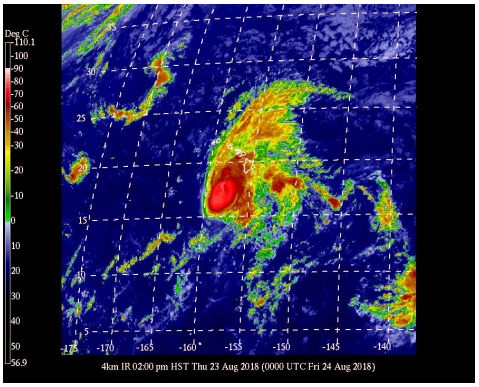

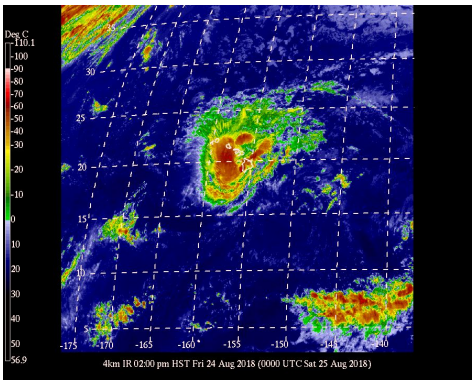

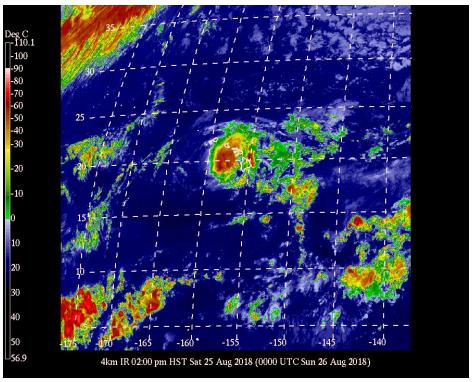

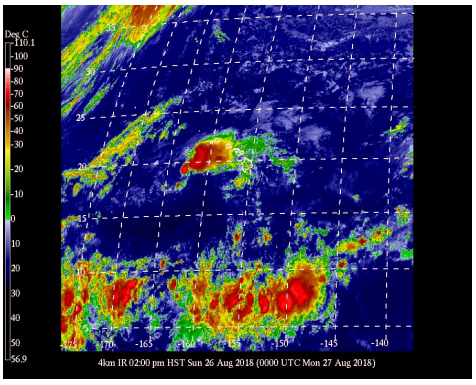

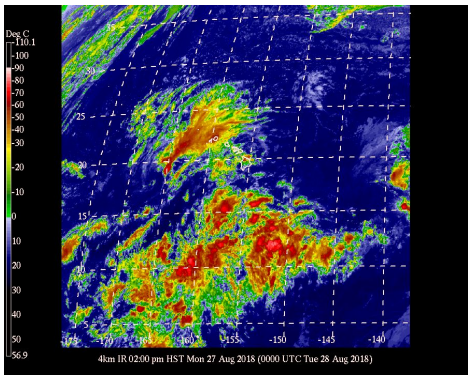

Figure 6: 4 km infrared satellite imagery from GOES 15 of Hurricane Lane on 00z from August 22 -27 viewed from top to bottom and left to right. The brighter colors (reds and oranges) indicate lower temperatures and thus higher cloud tops. Lane can be viewed at Category 5 intensity (top left) decaying to a tropical storm (bottom right). Obtained from http://weather.hawaii.edu.

b. Storm Precipitation

Radar precipitation accumulations from August 21-27 show many locations across the Hawaiian Islands islands receiving over 508 mm of rain from Lane (Figure 7a). High rainfall totals (radar derived precipitation accumulations >508mm) are found on the islands of Kauaʻi, east Maui, and Hawaiʻi island. Radar derived rainfall accumulation from August 22-26 had a maximum of 1107 mm on the windward side of the Hawaiʻi Island (Figure 7b). Rain gauge precipitation totals over this same period are generally consistent, also showing high precipitation accumulations on the eastern side of Hawaiʻi Island (Figure 8a).

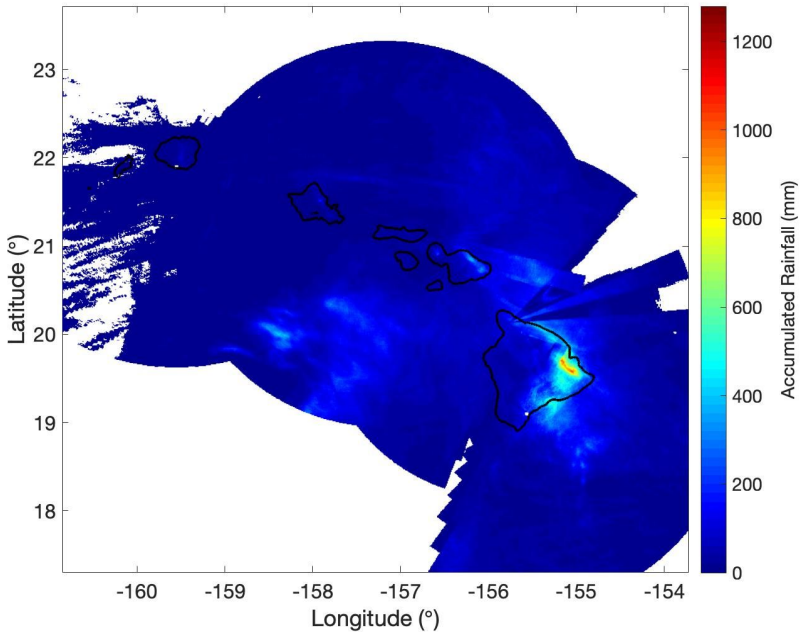

A

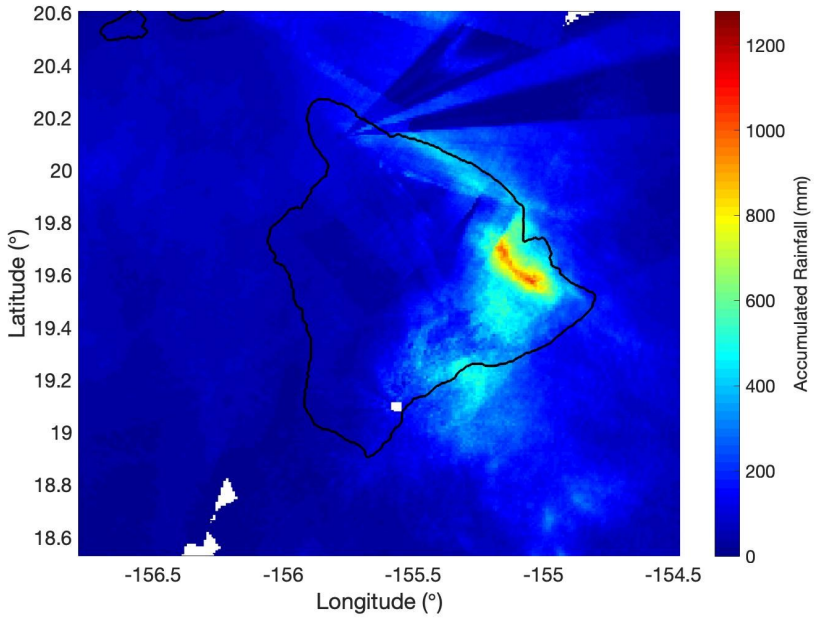

B

Figure 7: (a) Radar derived rainfall accumulation (mm) from Aug 22-27, 2018 HST for the entire Hawaiian Island chain and zoomed in to just (b) Hawai‘i Island for the same time period. Rain accumulations are derived from all four operational radars using LROSE.

Five rain gauges with the largest rainfall accumulations from August 22-25 on the eastern (windward) side of Hawai‘i Island are plotted in Figure 8b. These include Mountain View (MTVH1 19.5490 °N 155.1101 °W) which received 1293 mm of rain over this time period as well as Pi‘ihounua (PTTH1 19.7098 °N 155.139° W), Hilo (HTO 19.72 °N 155.04 °W), Waikea Uka (WKAH1 19.658 °N 155.1277 °W), and Pahoa (PHAH1 19.5406 °N 155.972 °W) with rainfall totals ranging from 929 mm to 1215 mm (Figure 8b). Significantly lower rainfall totals were observed by rain gauges and radar on the western (leeward) side of Hawai‘i Island.

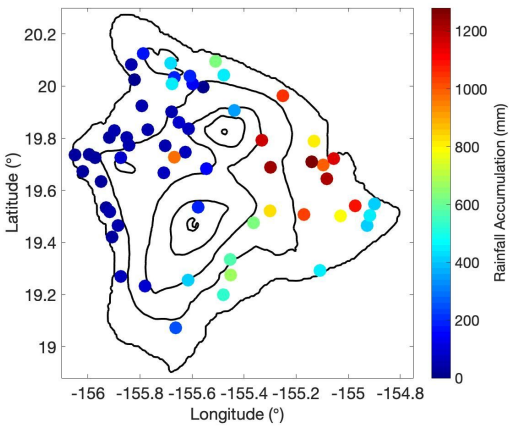

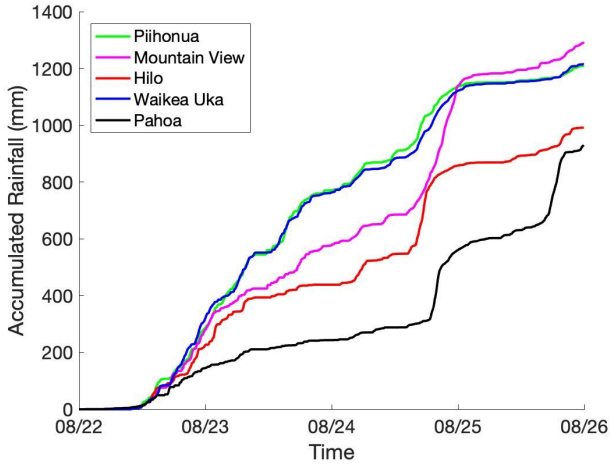

Figure 8: (a) Rain gauge rainfall accumulation (mm) from August 22-25, 2018 HST from all available stations across Hawai‘i Island. Terrain contour intervals are included every 1,000 m and (b) time series from the five highest accumulating rain gauge stations over this same time period (locations shown in Figure 2).

Figure 8b highlights that rainfall on the windward side of the Hawai‘i Island began in the afternoon of August 22 local time. Rainfall steadily accumulated until August 26 with 280 mm of rain on August 22, 301 mm on August 23, and a big rainfall event of 565 mm on August 24 followed by 156 mm on August 25 as measured by the Mountain View (MTVH1 19.5490 °N 155.1101 °W) rain gauge.

Another way to view rainfall through time is with a Hovmoller diagram; a spatial time series of radar-derived rain rate from the South Point (PHWA) radar is shown in Figure 9. Steady rain rates are observed by the radar on August 22-23, with a period of intense rainfall over higher terrain beginning later in the day on August 24 into the 25th, and another burst later on the 25th closer to the coastline (indicated by the red vertical line). From Figure 9, one can see that at early times during Lane (Aug 22), precipitating showers moved from east to west, consistent with the low level wind direction. But at later times (Aug 24-25), precipitation was widespread and sometimes moved west to east. Low level wind directions verified from the 925 mb sounding level and upstream wind direction from reanalysis data.

Within the multi-day Lane event, precipitation during a shorter period of the storm was a focus. The period from 3pm to 11pm HST on August 22 was chosen because of the prevailing synoptic wind direction, which was similar to trade wind flow. Results from the reanalysis model data shows that the winds at 925 mb to the east of Hawai‘i Island at 06z were ENE at 58°. The precipitation in this period therefore had the potential to be orographically enhanced as is common with trade wind showers (Esteban and Chen 2008). Focusing on a small time period within the 96 hour-long event gives us a better understanding of the imbedded smaller rain events and rainfall processes associated with it.

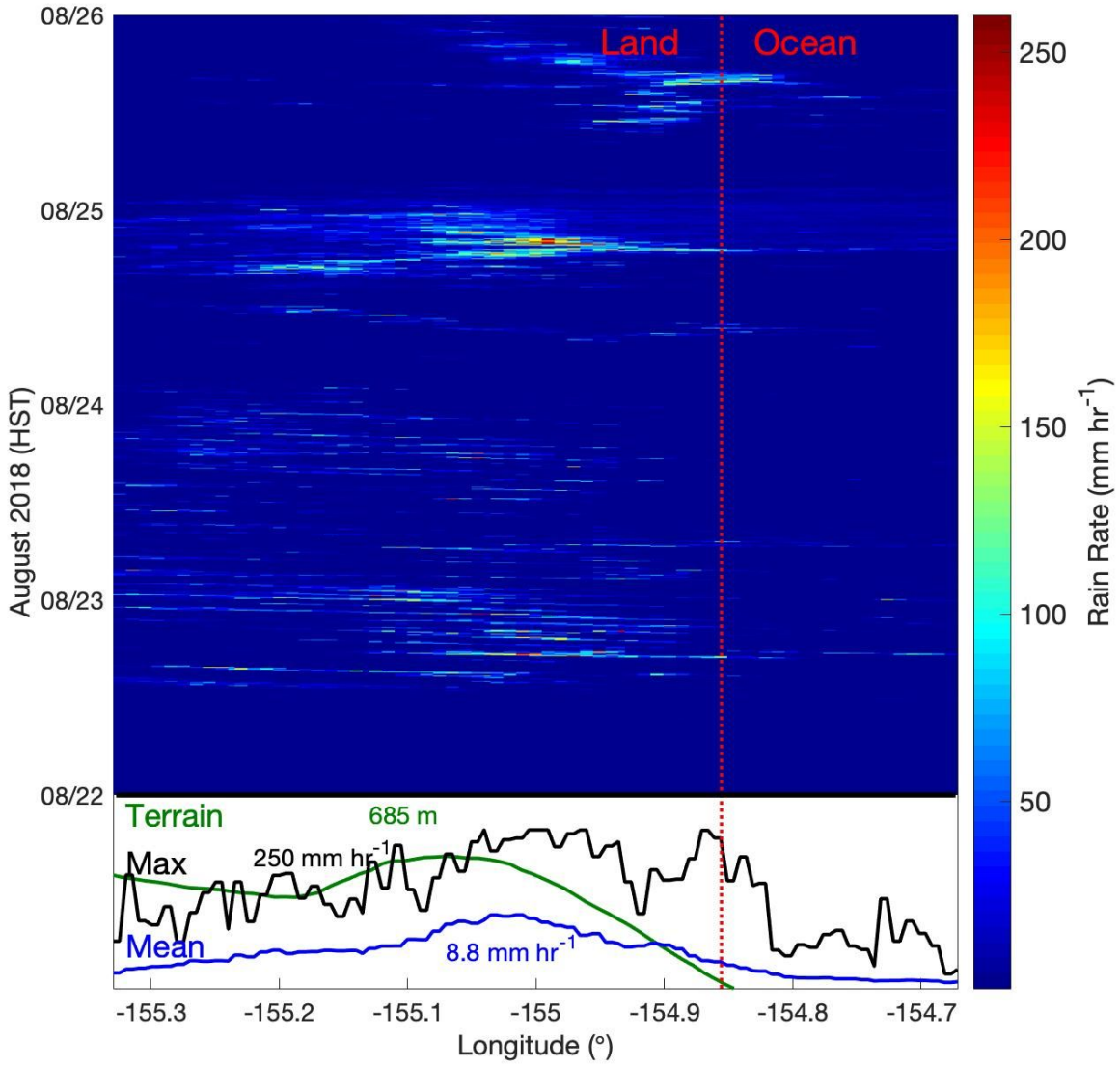

Figure 9: A hovmoller diagram along the Hov Line in Figure 2 showing radar derived rain rates (in hr^{-1})from August 22-August 25 HST. The red dotted line indicates the location of the coastline. Right of the line is ocean and left of the line is land. The green line at the bottom indicates terrain height along the latitudinal Hov line. The blue line at the bottom indicates the average rain rate (mm hr^{-1}) for the entire 96-h period with longitude corresponding to the HOV diagram. The black line indicates maximum rain rate (mm hr^{-1}) for the entire 96-h period

with longitude corresponding to the HOV diagram.

c. Focusing in on August 22, 2018

On August 22, the outer rainbands of Lane were approaching Hawai‘i Island's southeastern coast, evident in satellite imagery (Figure 6). The Hilo sounding (Figure 10) launched at 06z on August 23 (August 22 8pm HST) showed a wind direction at 925 hPa of 85-90°, calculated 259.8 J kg^{-1} of convective available potential energy (CAPE), and 61.46 mm of precipitable water (PWAT). The sounding also calculated t level of free convection (LFC) at 899.6 mb , and the Lifting Condensation Level (LCL) at 963.2 mb. The wind direction at coastal surface wind stations south of Mountain View showed similar 85-90° wind directions at low levels at this time. Also from the ECMWF IFS CY41r2 model on August 23 06z had an average wind direction of 58° and wind speed of 6 m s^{-1} at 925 mb upstream of the island (not shown).

The Hilo sounding from 0z, and 06z on August 23rd (2pm, 8pm August 22 HST) showed a saturated moist-neutral environment at nearly all levels (Figure 10).

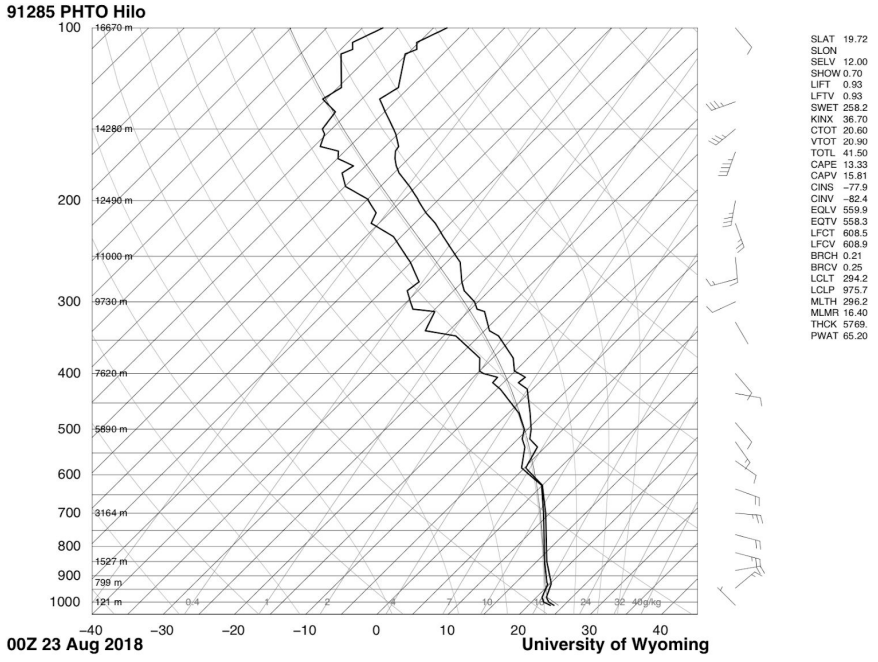

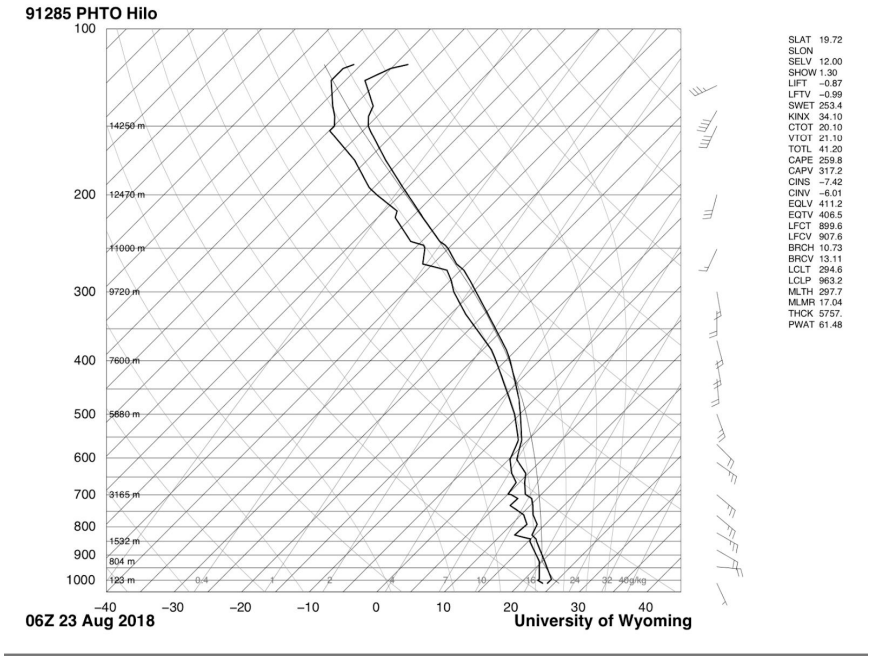

Figure 10: The Hilo sounding from Aug 23 at 00z (left) and 06z (right) plotted on a Skew-T ln-P graph, obtained from: http://weather.uwyo.edu/upperair/sounding.html. The rightmost dark black line is Temperature, and the leftmost dark line is Dew Point Temperature. Altitude and pressure (m and hPa) are shown on the left-axis, and temperature (°C) is shown on the bottom axis. Wind barbs are included on the right-hand side with altitude.

Rainfall accumulations during an 8-h period on August 22 from 3pm to 11pm HST contributed 26.6% of the total storm rainfall on the windward side of Hawai‘i Island, bringing a maximum of 294 mm of rain to windward locations (Figure 11a). Rain gauge accumulations over this 8-h time period were similar to the radar derived estimations; Pi‘ihounua (PTTH1 19.7098 °N 155.139° W) received 171.45 mm, Mountain View (MTVH1 19.5490 °N 155.1101 °W) received 178 mm, and Waikea Uka (WKAH1 19.658 °N 155.1277 °W) received 235 mm (Figure 11b). Rainfall at the Waikea Uka rain gauge contributed 19.3% of the total accumulated rainfall at the gauge over the entire 4-day event duration.

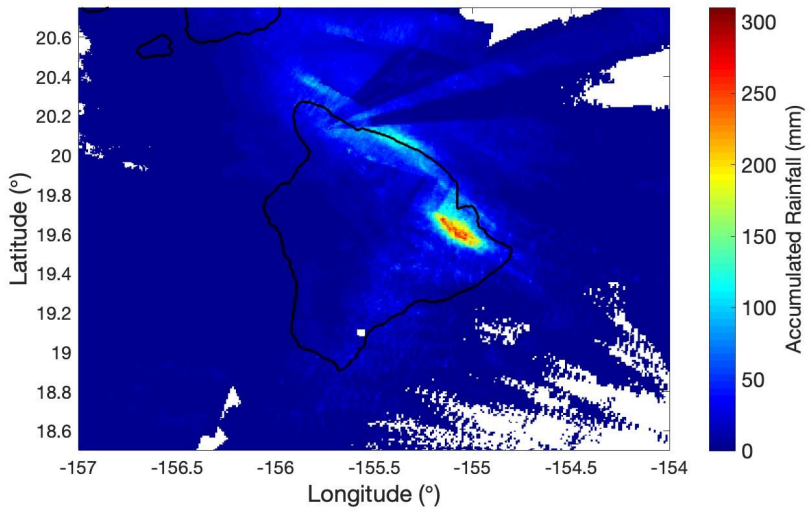

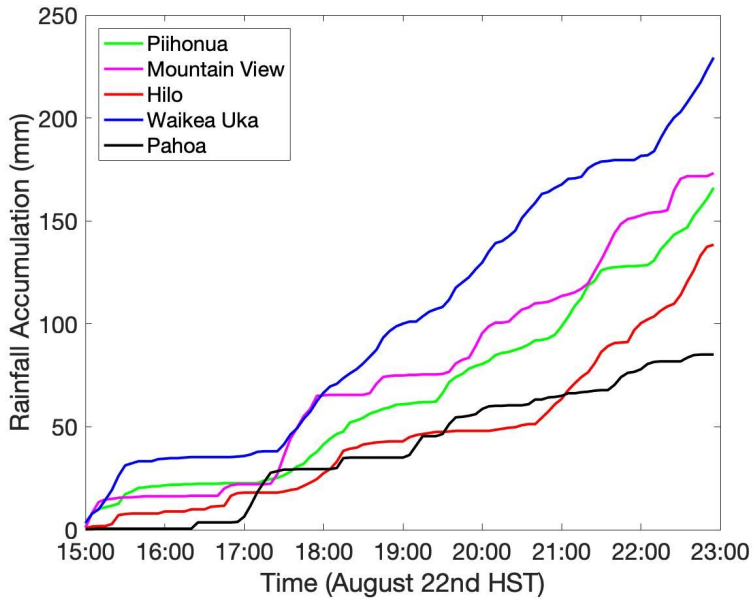

Figure 11: a) Radar derived rain accumulation (mm) on August 22, 2018 from 3 pm to 11 pm HST on Hawai'i Island and b) a time series of the cumulative rain gauge rainfall (mm) over this same time period. Gauge colors correspond to the locations in Figure 2.

d. Orographic Enhancement

A significant amount of rainfall fell on August 22, 2018 on the eastern portion of Hawai‘i Island while the winds were easterly. An important question arises: did the terrain of Hawai‘i Island play a role in the heavy rainfall? If the island were not there, would an open ocean location have received just as much? To answer this question, rainfall over the island was compared to rainfall just offshore over the ocean upstream. If the ocean and land locations received a similar amount of rain, heavily precipitating showers likely moved over land with the background flow, dropping rain along the way. However, if the land has more rainfall than the ocean, it is likely the terrain played a role in enhancing the showers.

To test the role of the orography, radar derived rain accumulations from the offshore ‘ocean’ box were compared to the ‘land’ box (Figure 12). The average rain accumulation for the ocean box over the 8-h period was 19.34 mm while the land box accumulated 85.6 mm over the same time period. This shows a 443% increase from the ocean to the land box, clear evidence of orographic enhancement as the precipitating showers moved from east to west with the background wind.

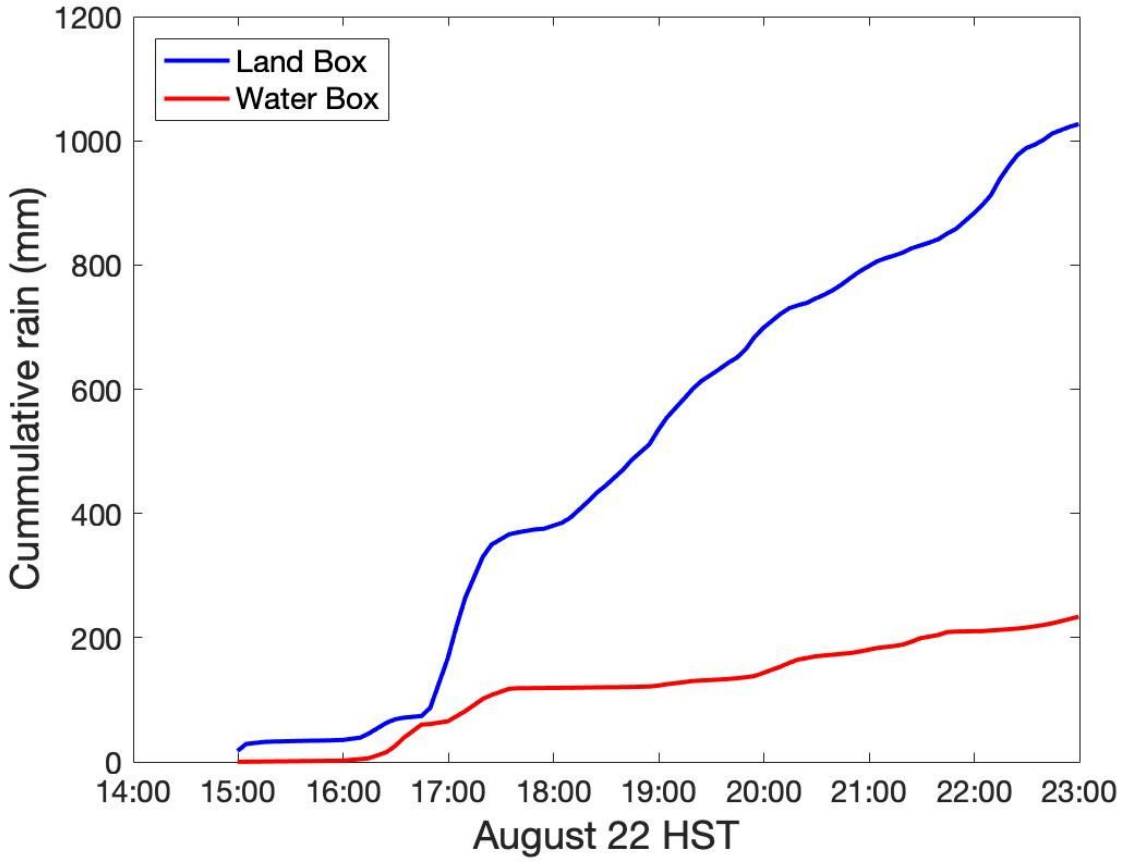

Figure 12: Radar-derived cumulative rainfall (mm) on August 22 from 3-11 pm HST. Average rain accumulation in the land (blue) and ocean (red) boxes in Figure 2 are calculated for each 5-min radar scan.

A hovmoller diagram focused on this shorter time period of interest also shows orographic enhancement of rainfall as the showers moved with the easterly flow. Figure 13 shows a hovmoller using the same Hov Line from Figure 2. Out over the ocean (right side of Figure 13), rain rates are relatively light but as the showers move onshore with the easterly flow (left toward the center of the figure), precipitation is initiated and rain rates increase. Also seen in Figure 13 is an increase in the average rain rate from right to left, and an increase in the

maximum rain rate from right to left, with both analyses peaking in the center of the Hovmoller where terrain height is the highest along this cross-section.

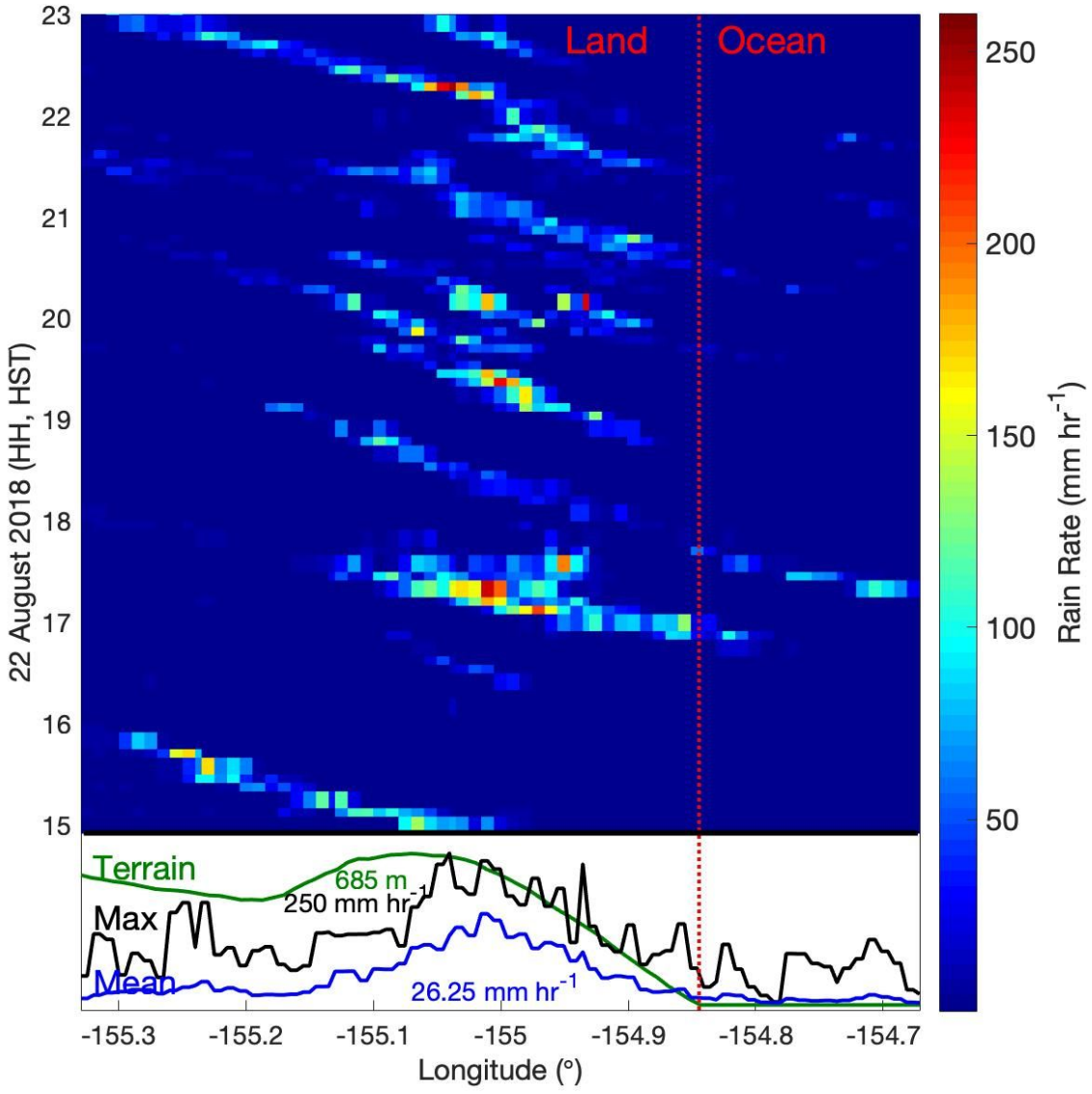

Figure 13: A hovmoller diagram along the Hov line in Figure 2 of radar derived rain rate from 1500 to 2300 HST on August 22, 2018. The red dotted line indicates the location of the coastline. Right of the line is ocean and left of the line is land. The green line at the bottom

indicates terrain height (not labeled) along the latitudinal Hov line. The blue line at the bottom indicates the average rain rate (mm hr^{-1}) for the entire 8-h period with longitude corresponding to the HOV diagram. The black line indicates maximum rain rate (mm hr^{-1}) for the entire 8-h period with longitude corresponding to the HOV diagram.

The enhancement of reflectivity (an indicator of rain rate) as showers move onshore can also be seen with a vertical cross-section from the radar along the same 'Hov' latitudinal line. Quasi range height indicator (RHI) plots in Figure 14 show the movement of a rain shower from east to west. The 6-panel figure shows cross-sections from 16:48 through 17:23 HST August 22 at 7-min increments. Reflectivity clearly increases as the rain shower moves westward. In Figure 14 panel 5, the reflectivity begins to weaken as the terrain height trends downward.

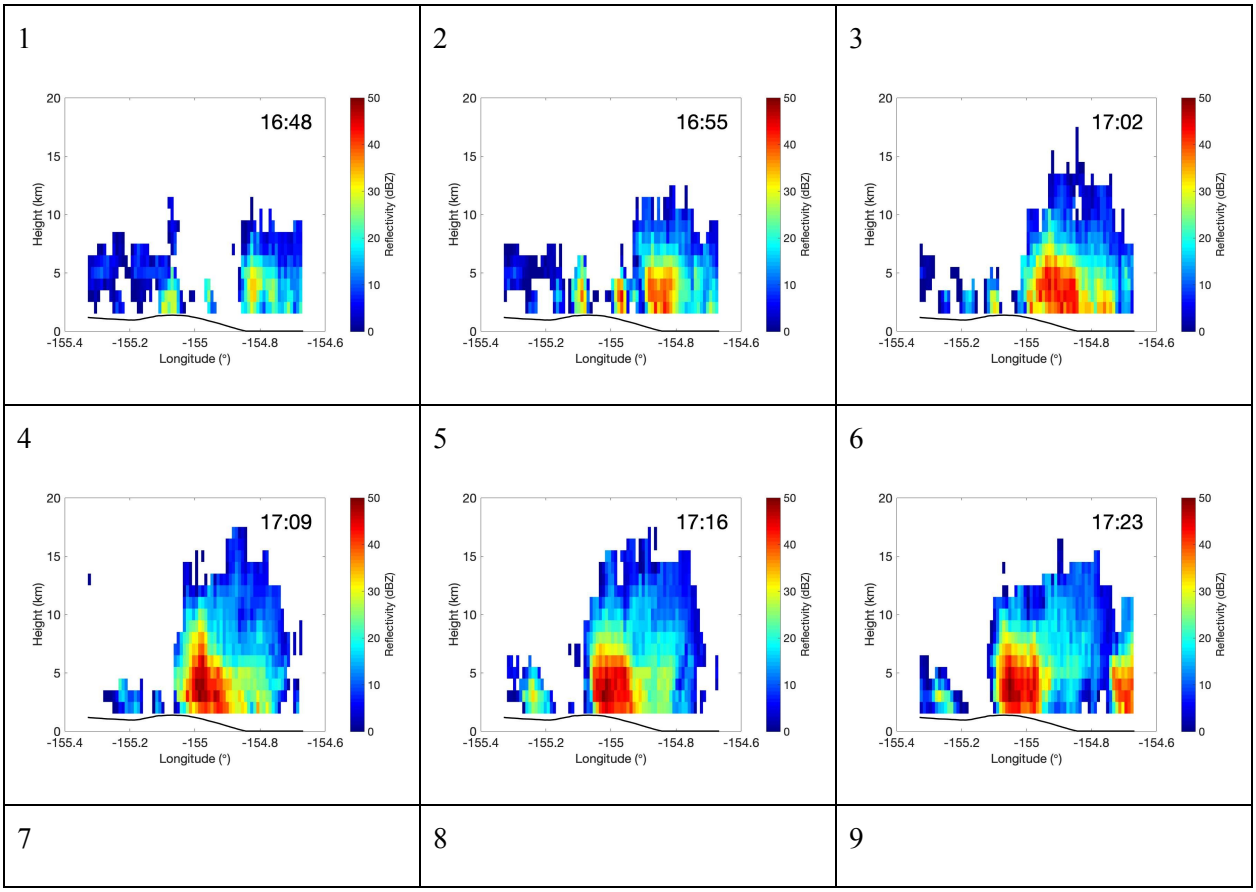

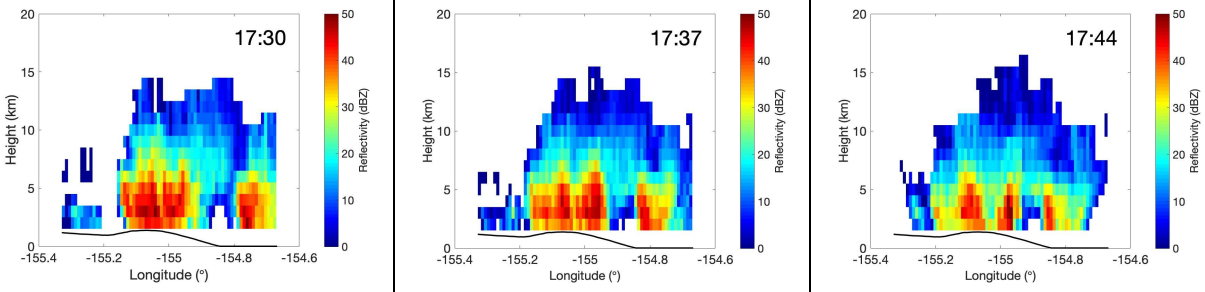

Figure 14: Vertical cross-sections across the Hov line in Figure 2 depicting reflectivity (dbz) with altitude. The 9-panels extend from 16:48 through 17:44 HST on August 22 from top to bottom and left to right. A black line at the bottom of each figure shows a proxy for terrain height.

As described in the introduction, heavy rainfall can come from long-duration low-intensity rainfall or from short-duration high-intensity rainfall. To test what mechanisms contributed to heavy rain from Lane, the duration and intensity of radar rainfall was analyzed. First, the maximum radar rain rates were analyzed for each grid point. Figure 15 shows that the area with maximum rain rates above 203 mm h^{-1} matches the location with the highest total accumulations in Figure 11a. Overall, maximum rainfall rates on land ranged from 50.8-250 mm h^{-1}. Figure 15 also shows that the highest rainfall rates were located near the windward shores of Hawai‘i Island. The southeast facing side of Mauna Loa and the northeast coast also had some high rain rates.

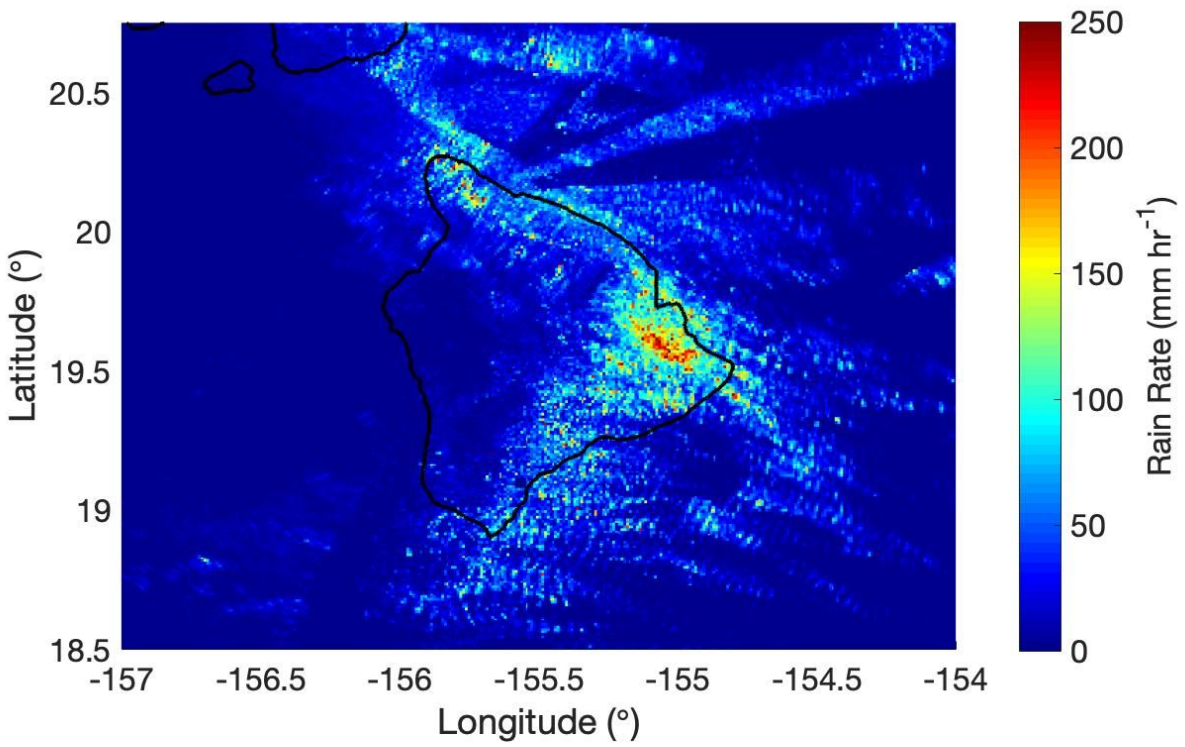

Figure 15: The maximum radar derived rain rate (mm hr^{-1}) for each grid point from any individual scan between 3-11 pm HST on August 22, 2018.

Another important detail that can be viewed from Figure 15 is the directionality of rain showers around and toward the island, especially on the south and east side of Hawai‘i Island. One can see heavily raining showers as quasi-linear features that stand out from the background, having been observed at a frequency of 7-min intervals over time. These quasi-linear features show that rain showers moved from east to west south of Hawai‘i Island near Honoka‘a and slightly south of east to slightly north of west to the east of Hawai‘i Island.

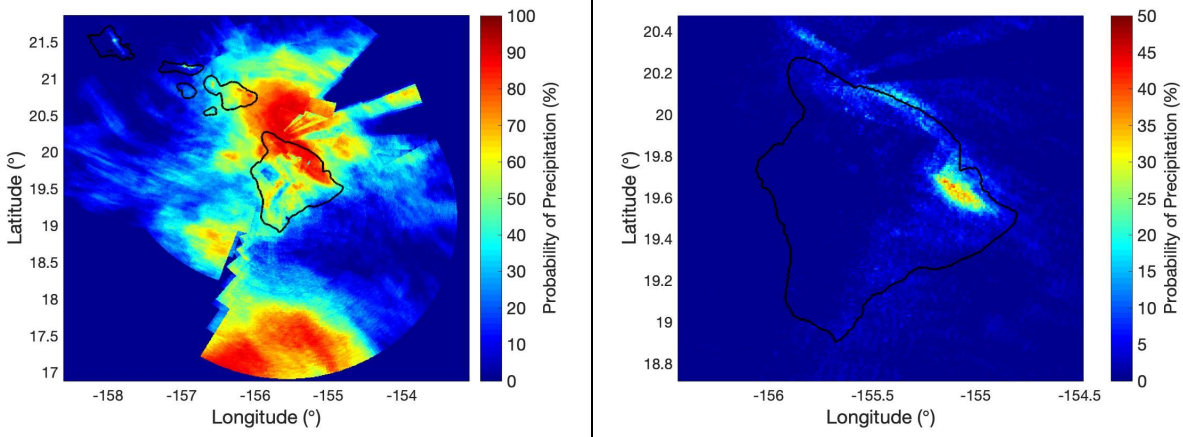

Figure 16: The probability (%) of rain rate > 0 mm hr^{-1} from radar from 3-11pm HST on August 22, 2018 and the probability of rain rate > 25.4 mm hr^{-1} from radar over the same time period. Note the change in color scale from 0-100% in a to 0-50% in b.

To quantify the duration of rainfall, the fraction of time raining was compared to the total amount of time in the period of interest (also known as the probability of precipitation, POP). The highest POP was found along the northeast coast of Hawai‘i Island (Figure 16), to the north, and well to the south of Hawai‘i Island. The region to the south is associated with the core of Lane. Performing the same calculation but for POP with rain rates > 25.4 mm hr^{-1} paints a completely different picture of the probability of heavy rain. The maximum POP is now associated with the Hilo area on the east side of Hawai‘i Island. Meanwhile, the probability in the Honoka‘a area on the northeast coast of Hawai‘i Island reduced significantly from near 100% to near 5%. In the 8-h time period, the POP >25.4 mm hr^{-1} was 50% on the windward side meaning 50% of the radar scans from 3 to 11pm had rain rates greater than 1 inch per hour. The POP of heavy rain rates elsewhere was well below 15% showing that the high POP initially seen for any measurable precipitation was dominated only by very small rainfall rates.

4. DISCUSSION & CONCLUSIONS

a. Factors leading to Extreme Precipitation

Extreme precipitation can come from long duration light rain, short duration heavy rain, or a combination of the two. With this in mind, the northeast side of Hawai‘i Island had nearly continuous rain over 85% of the time in an 8-hour duration when the threshold rain rate was 0 in hr^{-1}. Over the open ocean, two regions had nearly continuous rain, also at a low threshold rain rate: the ‘Alenuihāhā channel (between Maui county and Hawai‘i Island) and in the inner bands of Lane (Figure 16). When the rain rate threshold was increased to 25.4 mm hr^{-1}, the probability of rain > 25.4 mm hr^{-1} had a maximum in the Hilo and Mountain View areas on the east side of Hawai‘i Island (Figure 16). This matched closely with the 8-h accumulation total during the same time showing that continuous rainfall in other regions resulted only in modest accumulations due to low intensity, while the Hilo region experienced both high intensity and long duration leading to heavy rainfall accumulations.

The maximum rain rates across Hawai‘i Island showed an enhancement as rain cells moved upwind onto the land (Figure 13). A few storm cells peaked near the coastline offshore, but a majority were enhanced as they moved onshore, up the terrain on the windward side of the island. Figure 12 shows a 443% enhancement over land as compared to ocean during the 8-h period of interest. This provides strong evidence of orographic enhancement.

While orographic enhancement seems more than likely since rainfall accumulation is higher on land than over water, the question remains: why was precipitation enhanced in the Hilo region, but apparently not significantly enhanced elsewhere? Given the wind direction and terrain of Hawai‘i Island, one might expect precipitation to be enhanced along the entire windward coastline. Multiple factors may have contributed to the localized extreme precipitation from Lane. These factors are described in the following sections, and include 1) the general storm environment from Lane including its movement, 2) the terrain on the windward

side of Hawai‘i island and 3) the combined rainband placement and katabatic flow from Hawai‘i Island.

i. Storm Environment & Hurricane rainband convergence

Precipitation on Hawai‘i Island at the onset of Lane moved from east to west. Lane brought up to 234.6 mm of rain during the 8 hr period on August 22 as it approached the islands. The storm environment and the location of Lane were likely important factors for the heavy rainfall totals.

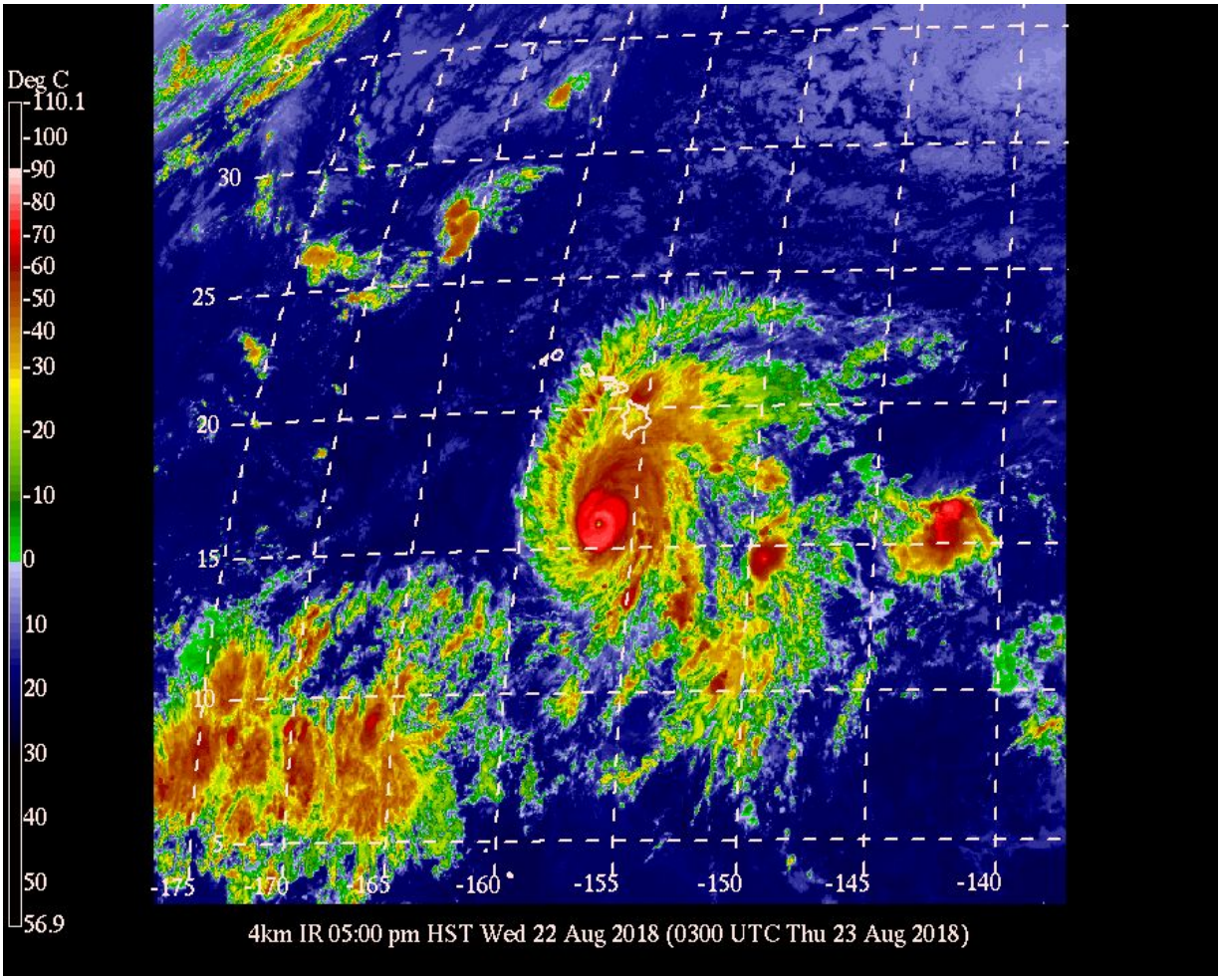

Figure 17: GOES-15 IR imagery at 4 km resolution on August 23 at 0300 UTC (August 22

1700 HST). Obtained from http://weather.hawaii.edu. Note the location of the hurricane rainbands.

Results from this study show that many individual convective cells contributed to high rainfall totals on the east side of Hawai‘i Island on August 22, 2018 HST. Satellite imagery at this same time show cloud top temperatures of -60°, indicating a strong possibility of the convergence band of the storm actively moving over the southeast portion of Hawai‘i Island.

When Lane was located west of Kona and south of Honolulu on August 22, it was moving slowly northward at 3.57 m s^{-1} (Powell 2018). The movement of Lane and the storm's rotation would cause the rainbands to move, albeit fairly slowly. Lane's cyclonic circulation and location suggests that Hawai‘i Island was receiving easterly winds in the low to mid levels of the atmosphere (950-700 hPa). The winds were verified with wind stations and reanalysis data during the period of interest. The rotation of the outer rainbands moving over the terrain brought with it an atmosphere with high moisture content 61.46 mm of precipitable water (Figure 10).

The storm environment set Hawai‘i Island up to have two important ingredients for heavy rainfall: moisture and surface convergence. With these ingredients in place, the terrain appears to have further enhanced the rainfall. Figure 14 shows the enhanced reflectivity rates of a rain cell increasing from 20 to 50 dbz from 4:48 pm HST to 5:23 pm HST as it moved into higher elevation.

ii. Terrain Enhancement

The onset of the storm brought low rainfall rates and an average accumulation of 19.3 mm offshore (Figure 12). As the rain bands moved westward with the easterly winds, the rain rates were enhanced by >400% over terrain to an average accumulation of 85.59 mm. Figure 14 depicted how the rain moved into and interacted with the terrain. Reflectivity values increased to up to 50 dbz moving up the terrain.

Figure 13 is an important figure for analyzing the possibility of orographic enhancement. If there is orographic enhancement, rain rates should increase going up the terrain based on the low level wind direction. It showed that the maximum rain rate increased with increasing

elevation. The terrain enhanced the maximum rain rates up to 250 mm hr^{-1}, and as the rainband moved down the terrain after the elevation peaked, there was a drop off in rain rates.

According to the upslope flow mechanism (Figure 1a and b), a preexisting cloud passing over the terrain produces a maximum of precipitation upwind of a barrier within a stable or unstable atmosphere. The vertical cross-sections (Figure 14) also clearly depict rain rates increasing with the terrain height. Figure 13 showed that each rain cell is independent from one another, but as they moved up the terrain in this 8-hr period, all experienced increased rain rates.

The preexisting cells in the coastal waters also reach the slope as they moved in with the synoptic background flow. This moved the storm cells up the terrain, and according to Chen and Nash 1994, cells that move up the terrain have a high probability of becoming orographically enhanced.

With the average easterly wind direction throughout the 8-h period, upslope flow is likely (Figure 1a and b). The moist neutral atmosphere (Figure 10) suggests stable upslope flow while the convective showers (Figure 14) suggest unstable upslope flow corresponding with figure 1b. CAPE values on August 23 00z and 06z remained small and stable at 13 J kg^{-1} and 259 J kg^{-1} while the atmospheric profile remained moist with PWAT of 65.02 and 61.46 mm (Figure 10).

Figure 13 shows that rain rates decreased as elevation began to decrease toward the west. This could be a real signal, or it could be a result of beam blockage (Figure 4) at 1.5 km where 50-60% of the beam is blocked by terrain. I cannot eliminate the possibility that due to the complexity of the terrain, the radar may not be able to measure accurate rain rates. It is seen that some precipitation was advected over the hilltop and not evaporated by descent over the leeside; Figure 13 showed rain rates above 100 mm on the western side of the Hov line.

Seeder feeder mechanisms (figure 1f) may be thought to have played a factor. This mechanism has been observed in hurricane-terrain interactions in the past (Smith et al. 2009) but at this time cannot be proven or disputed from the study due to the lack of cloud observations.

The orographic enhancement mechanism is characterized by enhanced rainfall from pre-existing showers that move over a terrain feature (figure 1e). Enhancement of pre-existing rainfall can be seen in Figure 13, where rainfall, likely from Lane's convergence band, exists upwind of the coastline and reflectivities are increased as the showers more onshore.

Another aspect to consider is that the direction of the wind field and sounding variables also determine the location of maximum precipitation. Past studies (e.g. Kodama and Barnes 1997) showed the southeast Mauna Loa area should receive more rainfall with southeasterly flow. However, the synoptic scale winds showed a more easterly component (Figure 10), and the wind stations (KMOH1 19.2927 °N 155.1075 °W, PLIH1 19.3175 °N 155.29 °W) near Kalapana showed the easterly winds splitting around Hawai‘i Island during this time period (not shown). As for sounding variables, although the 06z sounding was very moist with PWAT of 61.46 mm, the CAPE was 259 J kg^{-1}, showing little instability aloft. For heavy precipitation to occur on the southeast side of Mauna Loa, higher instabilities would be expected.

iii. Katabatic Flow

One last possible orographic enhancement mechanism that may have contributed to the rainfall during the 8-hr period of interest was katabatic flow. Figure 15 and 16 show some rain focused offshore along the windward coast. Oftentimes there is convergence offshore on the windward side of Hawai‘i Island due to orographic blocking (Chen and Nash 1994) causing the airflow to slow down as it approaches the terrain. The effects of orographic lifting aloft are enhanced by the nighttime convergence east of Hilo due to the interaction between the katabatic-land-breeze flow and the trade winds. The progression of the onset of katabatic flow down the slope is held up near the coast because the region is more exposed to the trade wind flow (Chen and Nash 1994). This could explain why in Figure 15, spots near the windward coast had rain rates >177.8 mm hr^{-1}.

Katabatic flow corresponds to Figure 1d, where the nighttime cooling over the higher terrain suppresses convection (Houze 2012). According to the windward wind stations, wind speeds in the Hilo area remained variable throughout the evening to night time hours due to orographic blocking and local modification. Due to the light and variable winds, land-sea temperature gradient, and rain evaporative cooling, the katabatic flow may have contributed to the rainfall near the coast. Rainbands often form at the convergence line between the offshore flow from the mountains and the incoming trade wind (Carbone et al. 1995). Past studies show

that if this is occurring, the region of maximum rainfall frequency should move seaward (Chen and Nash 1994).

The wind station between Mauna Loa and Mauna Kea showed westerly wind throughout the event but a look at its long term data shows that the station is not trustworthy. Due to the limited amount of accurate observational datasets, I can only speculate for this specific event. Other studies done (Chen and Nash 1994) have shown that the katabatic flow offshore plays a role in Hawai‘i islands’ rainfall specifically during periods of trade winds.

b. Summary

Hurricane Lane brought large amounts of rainfall to Hawai‘i Island. A number of different ingredients and factors likely played a role in the observed precipitation totals. Radar shows derived precipitation at a higher spatial and temporal resolution than the rain gauge network and was advantageous for observing rainfall over the open ocean. It was hypothesized that rain from Lane was orographically enhanced by the topography of Hawai‘i Island. This hypothesis was tested by focusing on an 8-hr period of interest from 3-11pm on August 22, 2018. This period constituted 26% of the 4-day total rainfall from Lane (Figure 11). Results from our analysis strongly suggest that rain during the 8-h period of interest was enhanced by terrain. Rainfall over land was 443% greater than that over an equivalent size ocean area directly offshore to the east upstream (Figure 12). A horizontal cross section matching the synoptic wind flow was created to analyze the precipitation as it moved onto shore and up the terrain. Individual precipitating showers grew in height and intensity as they lifted over the island mountains with a maximum of 250 mm hr^{-1} near the peak of elevation (Figure 13). The area that received the highest accumulation within the 8-hr period had rain rates greater than 25.4 mm hr^{-1} over 40% of the time (Figure 14).

The exact mechanism for the enhancement remains unknown with limited observations, but a number of possible mechanisms were explored. The position of Lane was an important factor in where the rain bands were setup and how they interacted with the island topography. Heavy rainfall occurred on the terrain aspect that faced the storm wind. With high moisture

contents of PWAT of 61.46 mm, this type of situation clearly has the potential to bring intense rainfall over a long period of time. The terrain enhancement through different mechanisms were proven through figure 12 and 13 and mimicked Houze's orographic mechanisms (figure 1). Katabatic flow also can be a contributing factor to the rainfall near the coast with rain rates >177.8 mm hr^{-1}.

On average, one tropical system of depression strength or greater passes within 300 km of the Hawaiian Islands every two years (Kodama and Barnes 1997). Given the rarity, case studies such as Lane serve as excellent examples for future storms, helping to analyze different rainfall mechanisms that lead to heavy precipitation. Although the Hawaiian Islands are not impacted by a major hurricane every year, studies have shown that the probability of future tropical cyclone frequency may be increasing near the subtropical central Pacific including the Hawaiian Islands (Murakami et al 2013). Furthermore, studies have shown that with increasing global temperatures, tropical storms are likely to be wetter, posing increased risk of flooding (Knutson 2010). However, future hurricane projections are not simulated at grid spacings that resolve terrain features, so only broad conclusions can be made (Widlansky et al 2019).

REFERENCES

Barstad, I., & Smith, R. B. (2005). Evaluation of an Orographic Precipitation Model. *Journal of Hydrometeorology*, *6*(1), 85–99. https://doi.org/10.1175/JHM-404.1

Ballard, Robert (August 23, 2018). Hurricane Lane Discussion Number 34. *Central Pacific Hurricane Center* (Report). National Oceanic and Atmospheric Administration. Retrieved August 24, 2018.

Bergeron, T. (1965), On the low-level redistribution of atmospheric water caused by orography, paper presented at the International Conference on Cloud Physics, Tokyo and Sapporo, Japan, Int. Assoc. of Meteorol. and Atmos. Phys. of the Int. Union of Geod. and Geophys., 24 May to 1 June.

Bier, J. A., Armstrong, R. W., & of Hawaii at Manoa., U. (1983). *Atlas of Hawaii / Department of Geography, University of Hawaii ; [editor and project director, R. Warwick Armstrong ; cartographer, James A. Bier]*(2nd ed.). University of Hawaii Press Honolulu.

Bringi, V. N., T. D. Keenan, and V. Chandrasekar, 2001: Correcting C-band radar reflectivity and differential reflectivity data for rain attenuation: A self-consistent method with constraints. IEEE Trans. Geosci. Remote Sens., 39, 1906–1915.

Carbone, R. E., W. A. Cooper, and W.-C. Lee, 1995: Forcing of flow reversal along the windward slopes of hawaii. *Monthly Weather Review*, 123 (12), 3466–3480, doi:10.1175/1520-0493(1995) 123⟨3466:FOFRAT⟩2.0.CO;2

Chen, Y.-L., and A. J. Nash, 1994: Diurnal variation of surface airflow and rainfall frequencies on the island of hawaii. *Monthly Weather Review*, 122 (1), 34–56, doi:10.1175/1520-0493(1994)122⟨0034:DVOSAA⟩2.0.CO;2,

Chen, Y.-L., & Nash, A. J. (2002). Diurnal Variation of Surface Airflow and Rainfall Frequencies on the Island of Hawaii. *Monthly Weather Review*. https://doi.org/10.1175/1520-0493(1994)122<0034:dvosaa>2.0.co;2

Chen, Y.-L., & Feng, J. (2002). Numerical Simulations of Airflow and Cloud Distributions over the Windward Side of the Island of Hawaii. Part I: The Effects of Trade Wind Inversion*. *Monthly Weather Review*, *129*(5), 1117–1134. https://doi.org/10.1175/1520-0493(2001)129<1117:nsoaac>2.0.co;2

DeHart, J. C., & Houze, R. A. (2017). Orographic Modification of Precipitation Processes in Hurricane Karl (2010). *Monthly Weather Review*, *145*(10), 4171–4186. https://doi.org/10.1175/MWR-D-17-0014.1

Doswell, C. A., H. E. Brooks, and R. A. Maddox, 1996: Flash flood forecasting: An ingredients-based methodology. *Weather and Forecasting*, 11 (4), 560–581, doi:10.1175/1520-0434(1996)011⟨0560:FFFAIB⟩2.0.CO;2,

Esteban, M. A., & Chen, Y.-L. (2008). The Impact of Trade Wind Strength on Precipitation over the Windward Side of the Island of Hawaii. *Monthly Weather Review*, *136*(3), 913–928. https://doi.org/10.1175/2007MWR2059.1

Giambelluca, T.W., Q. Chen, A.G. Frazier, J.P. Price, Y.-L. Chen, P.-S. Chu, J.K. Eischeid, and D.M. Delparte, 2013: Online Rainfall Atlas of Hawai'i. *Bull. Amer. Meteor. Soc.* 94, 313-316, doi: 10.1175/BAMS-D-11-00228.1.

Groisman, P. Ya., and Coauthors, 1999: Changes in the probability of heavy precipitation: Important indicators of climatic change. Climatic Change, 42, 243–283.

Hartley, T. M., & Chen, Y.-L. (2010). Characteristics of Summer Trade Wind Rainfall over Oahu. *Weather and Forecasting*, *25*(6), 1797–1815. https://doi.org/10.1175/2010WAF2222328.1

Haraguchi, P., 1977: Forecasting floods in hawaii (excluding hawaii island). *NOAA Tech. Memo. NWSSTM PR-16*, 30.

Hawaii 72 hour archive of the RR5HFO summary. *National Weather Service* (Report). National Oceanic and Atmospheric Administration. Retrieved February 8, 2019.

Houze, R. A., Jr., 2012: Orographic effects on precipitating clouds. Rev. Geophys., **50**, RG1001, doi:https://doi.org/10.1029/2011RG000365.

Hubbert, J., V. Chandrasekar, V.N. Bringi, and P. Meischner, 1993: Processing and Interpretation of Coherent Dual-Polarized Radar Measurements. J. Atmos. Oceanic Technol., **10**, 155–164, https://doi.org/10.1175/1520-0426(1993)010<0155:PAIOCD>2.0.CO;2

Karl, T. R., R. W. Knight, D. R. Easterling, and R. G. Quayle, 1996: Indices of climate change for the United States. Bull. Amer. Meteor. Soc., 77, 279–292.

Knutson, T.R., J.L. McBride, J. Chan, K. Emanuel, G. Holland, C. Landsea, I. Held, J.P. Kossin, A.K. Srivastava, and M. Sugi. 2010. Tropical cyclones and climate change.*Nature Geoscience* 3:157–163. February 21. doi:10.1038/ngeo779.

Knutti, R., and Coauthors, 2008: A review of uncertainties in global shigesato temperature projections over the twenty-first century. *J. Climate*, 21, 2651–2663, doi:10.1175/2007JCLI2119.1.

Kodama, K., and G. M. Barnes, 1997: Heavy rain events over the south-facing slopes of hawaii: Attendant conditions. *Weather and Forecasting*, 12 (2), 347– 367, doi:10.1175/1520-0434(1997)012⟨0347:HREOTS⟩2.0.CO;2.

Li, J., and Y.-L. Chen, 1999: A case study of nocturnal rain showers over the windward coastal region of the island of hawaii. *Monthly Weather Review*, 127 (11), 2674–2692, doi:10.1175/1520-0493(1999)127⟨2674:ACSONR⟩2.0.CO;2.

Lin, Y.-L., S. Chiao, T.-A. Wang, M. L. Kaplan, and R. P. Weglarz, 2001: Some common ingredients for heavy orographic rainfall. *Weather and Forecasting*, 16 (6), 633–660, doi:10.1175/ 1520-0434(2001)016⟨0633:SCIFHO⟩2.0.CO;2,

Longman, R.J., and Coauthors, *2018 Scientific Data*. Electronic dataset, University of Hawaii at Manoa

Maddox, R. A., C. F. Chappell, and L. R. Hoxit, 1979: Synoptic and mesoscale aspects of flash flood events. *Bulletin of the American Meteorological Society*, 60 (2), 115–123, doi:10. 1175/1520-0477-60.2.115.

Medlin, J. M., Kimball, S. K., & Blackwell, K. G. (2007). Radar and Rain Gauge Analysis of the Extreme Rainfall during Hurricane Danny's (1997) Landfall. *Monthly Weather Review*, *135*(5), 1869–1888. https://doi.org/10.1175/MWR3368.1

Murakami, H., Wang, B., Li, T., & Kitoh, A. (2013). Projected increase in tropical cyclones near Hawaii. *Nature Climate Change*, *3*(8), 749–754. https://doi.org/10.1038/nclimate1890

Murphy, M. J., & Businger, S. (2011). Orographic Influences on an Oahu Flood. *Monthly Weather Review*, *139*(7), 2198–2217. https://doi.org/10.1175/2010MWR3357.1

Nullet, D., & McGranaghan, M. (1988). Rainfall Enhancement over the Hawaiian Islands. *Journal of Climate*, *1*, 837–839. Retrieved from https://journals.ametsoc.org/doi/pdf/10.1175/1520-0442(1988)001%3C0837:REOTHI%3E2.0.CO;2

Powell, Jeff (August 22, 2018). Hurricane Lane Advisory Number 32 (Report). Central Pacific Hurricane Center. Retrieved August 23, 2018.

Roe, G. H., 2005: Orographic precipitation. *Annual Review of Earth and Planetary Sciences*,33 (1), 645–671, doi:10.1146/annurev.earth.33.092203.122541.

Romatschke, U., & Houze, R. A. (2011). Characteristics of Precipitating Convective Systems in the Premonsoon Season of South Asia. *Journal of Hydrometeorology*, *12*(2), 157–180. https://doi.org/10.1175/2010JHM1311.1

Secretaries of Commerce, Airforce, and Transportation. (2014). *Guidance on Adaptable Parameters Doppler Meteorological Radar* (Vol. 1).

Smith, R. B., Schafer, P., Kirshbaum, D., & Regina, E. (2009). Orographic Enhancement of Precipitation inside Hurricane Dean. *Journal of Hydrometeorology*, *10*(3), 820–831. https://doi.org/10.1175/2008JHM1057.1

Smith, R. B., Minder, J. R., Nugent, A. D., Storelvmo, T., Kirshbaum, D. J., Warren, R., … French, J. (2012). Orographic Precipitation in the Tropics: The Dominica Experiment. *Bulletin of the American Meteorological Society*, *93*(10), 1567–1579. https://doi.org/10.1175/BAMS-D-11-00194.1

Tu, C.-C., & Chen, Y.-L. (2011). Favorable Conditions for the Development of a Heavy Rainfall Event over Oahu during the 2006 Wet Period. *Weather and Forecasting*, *26*(3), 280–300. https://doi.org/10.1175/2010WAF2222449.1

Yu, C.-K., and L.-W. Cheng, 2008: Radar observations ofintense orographic precipitation associated with Typhoon Xangsane (2000). Mon. Wea. Rev., 136, 497–521, doi:10.1175/2007MWR2129.1.

Vivekanandan, J., Zrnic, D. S., Ellis, S. M., Oye, R., Ryzhkov, A. V., & Straka, J. (1999). Cloud Microphysics Retrieval Using S-Band Dual-Polarization Radar Measurements. *Bulletin of the American Meteorological Society*, *80*(3), 381–388. https://doi.org/10.1175/1520-0477(1999)080<0381:CMRUSB>2.0.CO;2

Wang, J.-J., & Chen, Y.-L. (2002). A Case Study of Trade-Wind Rainbands and Their Interaction with the Island-Induced Airflow. *Monthly Weather Review*, *126*(2), 409–423. https://doi.org/10.1175/1520-0493(1998)126<0409:acsotw>2.0.co;2

Wang, J.-J., & Chen, Y.-L. (2002). A Case Study of Trade-Wind Rainbands and Their Interaction with the Island-Induced Airflow. *Monthly Weather Review*, *126*(2), 409–423. https://doi.org/10.1175/1520-0493(1998)126<0409:acsotw>2.0.co;2

Widlansky, M. J., H. Annamalai, S. B. Gingerich, C. D. Storlazzi, J. J. Marra, K. I. Hodges, B. Choy, and A. Kitoh, 2019: Tropical Cyclone Projections: Changing Climate Threats for Pacific Island Defense Installations. Weather Clim. Soc., **11**, 3–15, https://doi.org/10.1175/WCAS-D-17-0112.1.

Woodard, C. J., Carey, L. D., Petersen, W. A., Felix, M., & Roeder, W. P. (2019). *Development and Testing of Operational Dual-polarimetric Radar Based Lightning Initiation Forecast Techniques*.

Xu, W., Zipser, E. J., Chen, Y.-L., Liu, C., Liou, Y.-C., Lee, W.-C., & Jong-Dao Jou, B. (2012). An Orography-Associated Extreme Rainfall Event during TiMREX: Initiation, Storm Evolution, and Maintenance. *Monthly Weather Review*, *140*(8), 2555–2574. https://doi.org/10.1175/MWR-D-11-00208.1

Zhang, J., Qi, Y., Langston, C., Kaney, B., & Howard, K. (2014). A Real-Time Algorithm for Merging Radar QPEs with Rain Gauge Observations and Orographic Precipitation Climatology. *Journal of Hydrometeorology*, *15*(5), 1794–1809. https://doi.org/10.1175/JHM-D-13-0163.1